The Fundamental Study on Ligand-Induced Green Fluorescent Protein UnaG and Its Applications

低分子依存性緑色蛍光タンパク質 UnaG の基礎的研究とその応用

February 2018

Waseda University
Graduate School of Advanced Science and Engineering
Department of Advanced Science and Engineering,
Research on Life Science and Medical Bioscience

Yoh SHITASHIMA
下島　洋

Contents

Chapter 1
General Introduction

1.1 Fluorescent Protein*

Fluorescent proteins (FPs) widely pervade to visualize the dynamics of biological phenomenon and act as fluorescent sensors, such as Ca^{2+}, pH, halide, and ATP concentration sensors [1-7]. Therefore, FPs are indispensable tools for various fields such as biochemistry, biophysics and cell biology. Since the *Aequorea victoria* green fluorescent protein (GFP) gene has been cloned [8] and been expressed in other species such as *Escherichia coli* [9], various improved GFPs have been engineered for utilizing as bio-imaging tools, like the expansion of the FP color palette and discoveries of GFP-like proteins from cnidarian and coral reefs. Enhanced GFP (EGFP), which could offer stronger brightness than wild-type GFP, was engineered as useful optical markers [10-12], These discoveries and improvements have made FPs more powerful as a good visualization tools of molecular-dynamic behavior in biological fields. Moreover, the recent discovery of ligand-induced fluorescent proteins (LIFPs), which acquires the fluorescent properties by binding exogenous fluorophore, promotes the applications of FPs.

The maturation of GFP-like fluorophores is very complicated. The specific tri-peptide (X-Tyr-Gly, X means any amino acid) in GFP or GFP-like protein (e.g. DsRed) forms fluorophore via three steps of chemical reaction, cyclization, dehydration and oxidation (Figure 1.1). When the environment around fluorophore changes via intentional alteration such as a site-directed mutagenesis or X in tri-peptide is specific amino acid (e.g. X in DsRed is Gln), the positional change of oxidation in tri-peptide occurs and induces a subsequent change of the length of conjugated system, and the resulting color variations of FPs. However, GFP-like proteins have two weak points. First, the maturation of fluorophore was too long, from several tens of hours to several days. Second, the fluorophore formation requires oxygen.

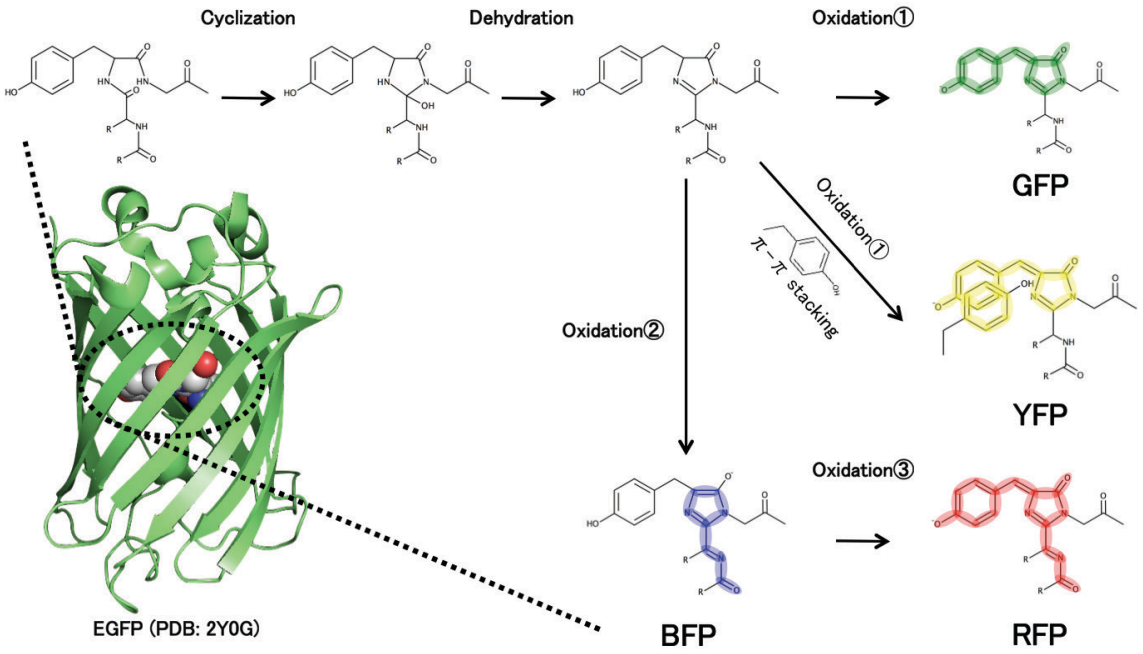

Figure 1.1. The fluorophore formation of *Aqueoria Victoria* GFP, the yellow mutant GFP (YFP), and red fluorescent protein like DeRed. This figure was based on A. Miyawaki, Syujun-sya, 2010 [13]. The cartoon image of EGFP was created using PyMol (DeLano Scientific) from PDB files 2Y0G.

Not only the fluorescence intensity (FI) but also the chromophore maturation is important for several biological applications [14], because rapidly maturing fluorescent proteins provide efficient fluorescence imaging, and therefore detail maturation rate of GFP and its mutants are reported [15]. Thus, applications of fluorescent protein as a useful probe are required for developments of bio-imaging technology. Recent developments of LIFPs have provided further options for researchers using FPs. LIFPs overcome the weak points of GFP-like proteins. For example, near-infrared LIFPs, such as IFP1.4, which utilize covalently bound biliverdin-related molecule [16, 17] surpassed the longer wavelength emission barrier of GFP-like fluorophores, leading to deep tissue/body live-cell imaging. Some LIPFs, like iLOV, utilize a non-covalently bound flavin-related

molecule [18, 19] and exhibit green fluorescence. FPs have features of instantaneous and oxygen-independent fluorophore formation, which the GFP family proteins do not have. Figure 1.2 shows the structure of biliverdin-binding fluorescent protein, the precursor of IFP1.4 (A) and flavin mononucleotide-binding fluorescent protein, iLOV (B). From such features, LIFPs have a potential of novel fluorescent tools instead of GFP family proteins and attract in various fields.

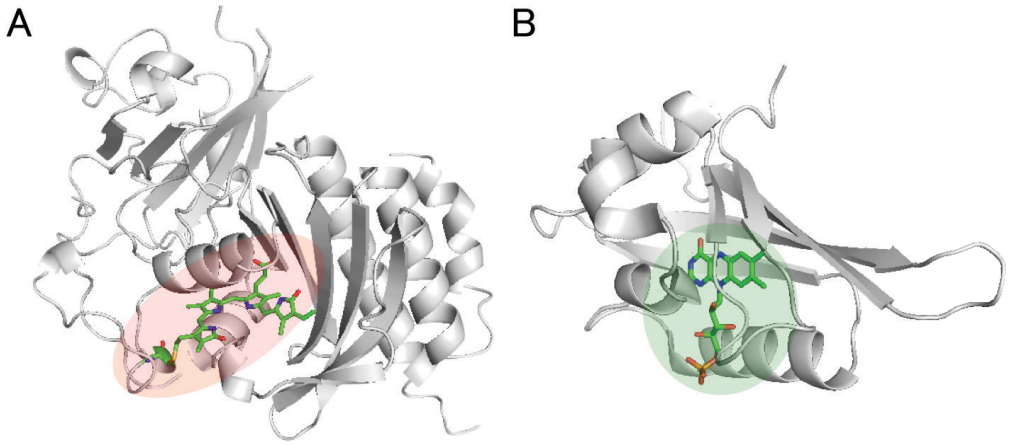

Figure 1.2. The protein structures of LIFPs. (A) The structure of DrCBD, which is the precursor of IFP1.4. (B) The structure of iLOV. Images were created using PyMol (DeLano Scientific) from PDB files 1ZTU and 4EET for (A, B), respectively.

---

* This section is reproduced with permission from Yoh Shitashima, Togo Shimozawa, Akiko Kumagai, Atsushi Miyawaki, and Toru Asahi, Two distinct fluorescence states of the ligand-induced green fluorescent protein UnaG, *Biophysical Journal*, 113, 2805-2814 (2017) [20], Elsevier, copyright 2017. Consent from all authors has been secured.

1.2 Fatty Acid Binding Protein

In this thesis, I focus on UnaG, which was recently discovered green LIFP in eel muscles. Before I describe UnaG, I explain the general introduction of fatty acid binding protein (FABPs) because UnaG is a member of the FABPs. One of the most important functional proteins, FABPs, which are classified various FABP types, like heart-type FABP (H-FABP), brain-type FABP (B-FABP) and epidermal-type FABP (E-FABP), behave as intracellular carriers for incorporating polyunsaturated fatty acids (PUFAs) into cells [21-24]. Moreover, FABPs have attracted interest as biomarkers because they also play physiological roles. For example, (i) H-FABP, which manages intracellular transport of free fatty acids in heart, can be an effective prognostic marker for heart failure and/or cardiovascular disease [25], and (ii) B-FABP has a potential role as biomarker for glioblastoma and/or dementia [26, 27]: because PUFAs are closely related with these diseases. Herein, FABPs play important roles to regulate intracellular behaviors of fatty acids (FAs) through the interaction between FABPs themselves and their ligands, PUFAs (dissociation constant, K_d = 10^{-7}~10^{-6} M) [28]. Hence, intentional change of ligand molecular interaction (e.g. binding affinity) would lead to regulating FAs' behaviors. UnaG belongs to FABP family with the highest homology to human B-FABP [29].

1.3 UnaG**

UnaG is a novel green LIFP discovered in eel muscles, is a first reported fluorescent protein derived from vertebrates, which is a superfamily of fatty-acid-binding protein (FABP) [29]. The apo state of UnaG (apoUnaG) high-specificity and -affinity binds bilirubin (BR) inside the β-barrel and forms the UnaG-BR complex (holoUnaG) (Figure 1.3). Due to the high-affinity of BR binding (K_d = 98 pM) [29] compared to other FABP holoprotein complexes, almost all UnaG in mammalian cell form holo state because of the abundance of BR in vertebrates. BR contains two dipyrrinone moieties (*endo*-vinyl and *exo*-vinyl dipyrinone), and both moieties absorb visible light from 400 nm to 500 nm, however, nobody knows which moieties contribute to exhibit fluorescence. Each dipyrrinone moiety has propionate and it forms many hydrogen bonds with UnaG. For instance, Arg132/Tyr134 residues anchor the *endo*-vinyl dipyrrinone propionate carboxylate, and Ser80/Asp81 residues attach to the propionate carboxylate from *exo*-vinyl dipyrrinone via a water molecule [29]. Hydrogen bonds in the former are seen in other FABPs, whereas those in the later are a particular feature in holoUnaG. This fact suggests that the anchored propionate carboxylate via Ser80/Asp81 residues bears the high affinity of BR binding [29].

The fluorescence spectrum and brightness of UnaG bound to BR (holoUnaG) are similar to those of EGFP [29]. The quantum efficiency (QE) of holoUnaG is ~50%, which is equivalent to that of EGFP, one of the brightest GFP mutants, although free BR in aqueous solution is almost dark, indicating that holoUnaG is bright enough to be detected in living cells. Additionally, the molecular weight of UnaG is 16.5 kDa, which is smaller than that of EGFP (27 kDa), indicating that UnaG can be useful tools for various fields. By utilizing the binding specificity to BR and the ligand-induced

fluorescence, quick measurements of indirect BR concentrations in blood have been reported as an application of UnaG [30]. Moreover, since the discovery of UnaG, it has been utilized for a fluorescent BR sensor [31] or a reversible fluorogenic protein-protein interaction reporter [32] in mammalian cells. Furthermore, it has also been utilized for a fluorescent hypoxia sensor [33] because UnaG can produces oxygen-independent fluorescence.

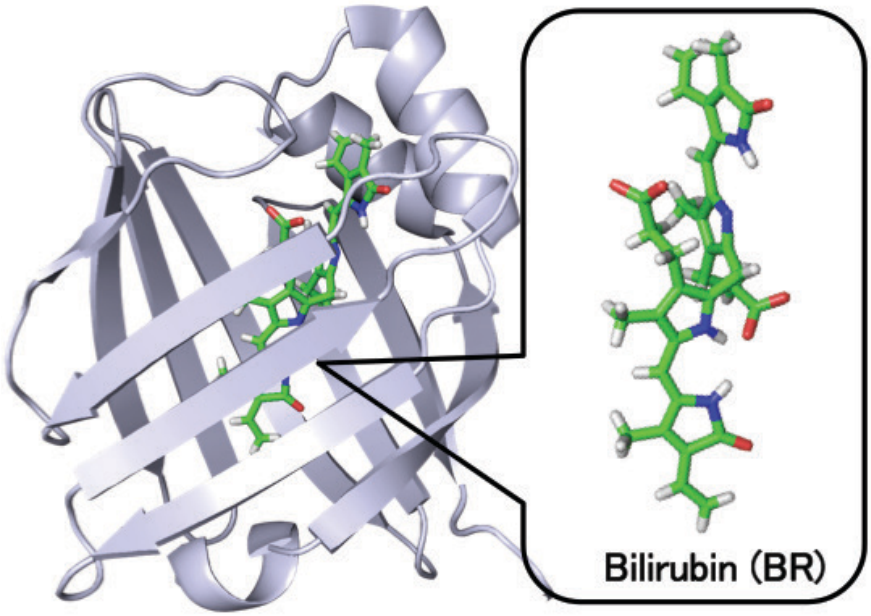

Figure 1.3. The structures of UnaG-Bilirubin complex. Image was created using PyMol (DeLano Scientific) from PDB files 4I3B.

** This section is reproduced with permission from Yoh Shitashima, Togo Shimozawa, Akiko Kumagai, Atsushi Miyawaki, and Toru Asahi, Two distinct fluorescence states of the ligand-induced green fluorescent protein UnaG, *Biophysical Journal*, 113, 2805-2814 (2017) [20], Elsevier, copyright 2017. This section is also reproduced with permission from Yoh Shitashima, Togo Shimozawa, Toru Asahi, and Atsushi Miyawaki, A dual-ligand-modulable fluorescent protein based on UnaG and calmodulin, *Biochemical and Biophysical Research Communications*, 496, 872-879 (2018) [34], Elsevier, copyright 2018. Consent from all authors has been secured.

1.4 Calmodulin

Calmodulin (CaM) is known as one of the most famous Ca^{2+} binding proteins and plays numerous physiological roles such as metabolism, apoptosis, muscle contraction, and nerve growth. CaM itself changes its conformational structure by binding to Ca^{2+} (Figure 1.4.), further Ca^{2+}-CaM complex drastically change its conformation by binding myosin light chain kinase fragment (M13), and this conformationally sensitive feature enables CaM to play various important cell functions. From the feature that CaM interacts with Ca^{2+} ion and resulting its conformational change, CaM has been utilized for genetically encoded fluorescent Ca^{2+} indicator[3]. Recently, various single fluorescent protein based indicators have been reported, indicating that CaM is still a useful conformational change receptor in protein engineering field. To genetically combine UnaG with CaM, I attempt to develop a novel application of UnaG.

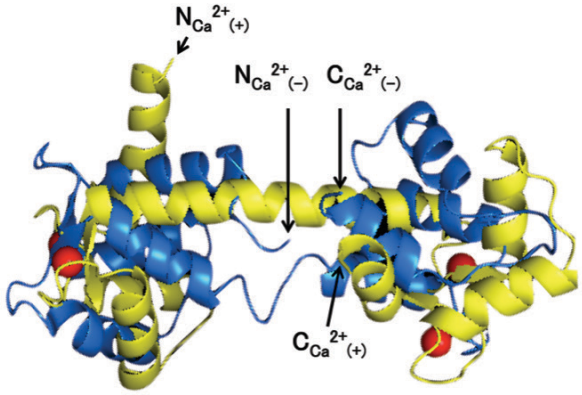

Figure 1.4. The crystal structure of CaM without Ca^{2+} (blue) and with Ca^{2+} (yellow). Ca^{2+} molecules are shown as red spheres. The alignment of both CaMs was performed using Pymol (DeLano Scientific) from PDB files 1CFD and 1CLL, respectively. $N_{Ca^{2+}(-)}$, and $C_{Ca^{2+}(-)}$, $N_{Ca^{2+}(+)}$, and $C_{Ca^{2+}(+)}$ indicated the N or C termini of CaM with or without Ca^{2+}, respectively.

1.5 Scope of this Thesis

In sections 1.3, I describe the feature and utility of UnaG. These previous reports imply that UnaG has a potential to be a compact fluorescent probe, which can be available in life science field. Despite the great potential of UnaG as a fluorescent probe, limited information of UnaG has hindered its application as a fluorescent probe. For example, the association/dissociation rate constants between UnaG and BR, which govern the fluorescence stability of protein, and the dispersion of UnaG in aqueous solution, which influences the functions of labeled proteins, are unknown. As an example of the former, if the dissociation rate is not negligible, frequent exchange of the ligand could prevent photo-bleaching [35, 36] and realize bright and stable fluorescent imaging even under conditions of high-intensity excitation light [37]. As an example of the latter, multimeric fluorescent proteins such as DsRed discovered in *Discosoma* sp. are difficult to use for bio-imaging because they may aggregate themselves through the interaction between fluorescent proteins [38]; therefore, monomeric DsRed were developed [39]. Moreover, although some previous reports have described the application of UnaG as BR sensors [30, 31, 33], the high affinity of UnaG itself and BR restrict these sensors to irreversible and one-time sensors. Additionally, the high affinity of ligand has hindered its utilization as a quantitative BR sensor *in vivo* because almost all UnaG in mammalian cell would form holo state and would exhibit the saturated fluorescence even if the concentration of BR is very low.

In this thesis, I have two purposes. First, I determined the important molecular properties of UnaG for utilizing this protein in life science fields. While analyzing the important molecular properties of UnaG such as the association and dissociation rates of ligand and the dispersibility of UnaG, I discovered two distinct fluorescence states in

holoUnaG. Two distinct fluorescence states and the reversible transition between two states is unique feature compared to other FPs. Second, I generated the novel UnaG/calmodulin chimeric protein which changes its binding affinity for bilirubin by calcium ion. The dual-ligand-controllable fluorescent protein that changes the affinity of BR binding depending on the Ca^{2+} concentration was generated by genetically insertion of calmodulin into UnaG.

This doctoral thesis contains four chapters. In chapter 1, I describe a general introduction of fluorescent protein, especially UnaG, and explain the purpose of this thesis. In chapter 2, the fundamental study on UnaG was described. I determined the dispersibility of UnaG, the association and dissociation rates of ligand, and two distinct fluorescence states in holoUnaG, and suggested a novel schema of the UnaG and BR complex system. In chapter 3, the application of UnaG was described. The calmodulin insertion around the BR binding pocket of UnaG provided a novel protein that regulates the affinity of BR binding by using Ca^{2+} ion. In chapter 4, I present a summary and future prospect of this thesis.

1.6 References

1. Chudakov, D. M., M. V Matz, S. Lukyanov, and K. A. Lukyanov, "Fluorescent proteins and their applications in imaging living cells and tissues", *Physiol. Rev.*, **90**, 1103–1163 (2010).
2. Mishin, A. S., V. V Belousov, K. M. Solntsev, and K. A. Lukyanov, "Novel uses of fluorescent proteins", *Curr. Opin. Chem. Biol.*, **27**, 1–9 (2015).
3. Miyawaki, A., and Y. Niino, "Molecular Spies for Bioimaging—Fluorescent Protein-Based Probes", *Mol. Cell.*, **58**, 632–643 (2015).
4. Llopis, J., J. M. McCaffery, A. Miyawaki, M. G. Farquhar, and R. Y. Tsien, "Measurement of cytosolic, mitochondrial, and Golgi pH in single living cells with green fluorescent proteins", *Proc. Natl. Acad. Sci.*, **95**, 6803–6808 (1998).
5. Miesenböck, G., D. A. De Angelis, and J. E. Rothman, "Visualizing secretion and synaptic transmission with pH-sensitive green fluorescent proteins", *Nature*, **394**, 192–5 (1998).
6. Jayaraman, S., P. Haggie, R. M. Wachter, S. J. Remington, and A. S. Verkman, "Mechanism and cellular applications of a green fluorescent protein-based halide sensor", *J. Biol. Chem.*, **275**, 6047–6050 (2000).
7. Berg, J., Y. P. Hung, and G. Yellen, "A genetically encoded fluorescent reporter of ATP:ADP ratio", *Nat. Methods*, **6**, 161–166 (2009).
8. Prasher, D. C., V. K. Eckenorde, W. W. Ward, F. G. Prendergast, and M. J. Cormier, "Primary structure of the *Aequorea victoria* green-fluorescent protein", *Gene*, **111**, 229-233 (1992).
9. Chalfie, M., Y. Tu, G. Euskirchen, W. W. Ward, and D. C. Prasher, "Green Fluorescent Protein as a Marker for Gene Expression", *Science*, **263**, 802-805

(1994).

10. Heim, R., and R. Y. Tsien, “Engineering green fluorescent protein for improved brightness, longer wavelengths and fluorescence resonance energy transfer”, *Curr. Biol.*, **6**, 178-182 (1995).

11. P. C, Brendan, R. H. Valdivia, and S. Falkow, “FACS-optimized mutants of the green fluorescent protein (GFP)”, *Gene*, **173**, 33-38 (1996).

12. A. G. C., Rlccardo, A. Ferrari, V. Pellegrini, M. Tyagi, M. Giacca, and F. Beltram, “The enhanced green fluorescent protein as a tool for the analysis of protein dynamics and localization: local fluorescence study at the single-molecule level”, *Photochem. Photobiol.*, **71**, 771-776 (2000).

13. A. Miyawaki, “Fluorescence Imaging Revolution”, Syujun-sya, 1st edition, 2010 (Japanese book).

14. Heim, R., A. B. Cubitt, and R. Y. Tsien, “Improved green fluorescence”, *Nature*, **373**, 663-664 (1995).

15. Iizuka, R., M. Yamagishi-Shirasaki, and T. Funatsu, “Kinetic study of de novo chromophore maturation of fluorescent proteins”, *Anal. Biochem.*, **414**, 173-178 (2011).

16. Shu, X., A. Royant, M. Z. Lin, T. A. Aguilera, V. Lev-Ram, P. A. Steinbach, and R. Y. Tsien, “Mammalian expression of infrared fluorescent proteins engineered from a bacterial phytochrome”, *Science*, **324**, 804–807 (2009).

17. Filonov, G. S., K. D. Piatkevich, L.-M. M. Ting, J. Zhang, K. Kim, and V. V Verkhusha, “Bright and stable near-infrared fluorescent protein for in vivo imaging” *Nat. Biotechnol.*, **29**, 757–761 (2011).

18. Drepper, T., T. Eggert, F. Circolone, A. Heck, U. Krauss, J.-K. K. Guterl, M.

Wendorff, A. Losi, W. Gärtner, and K.-E. E. Jaeger, “Reporter proteins for in vivo fluorescence without oxygen”, *Nat. Biotechnol.*, **25**, 443–445 (2007).

19. Shu, X., V. Lev-Ram, T. J. Deerinck, Y. Qi, E. B. Ramko, M. W. Davidson, Y. Jin, M. H. Ellisman, and R. Y. Tsien, “A genetically encoded tag for correlated light and electron microscopy of intact cells, tissues, and organisms” PLoS Biol., 9 (2011).

20. Shitashima, Y., T. Shimozawa, A. Kumagai, A. Miyawaki, and T. Asahi, “Two distinct fluorescence states of the ligand-induced green fluorescent protein UnaG”, *Biophys. J.*, **113**, 2805-2814 (2017).

21. Storch, J., and A. E. A. Thumser, “The fatty acid transport function of fatty acid-binding proteins”, *Biochim. Biophys. Acta - Mol. Cell Biol. Lipids*, **1486**, 28–44 (2000).

22. Zimmerman, A. W., and J. H. Veerkamp, “New insights into the structure and function of fatty acid-binding proteins”, *Cell. Mol. Life Sci.*, **59**, 1096–1116 (2002).

23. Schaap, F. G., G. J. Van der Vusse, and J. F. C. Glatz, “Evolution of the family of intracellular lipid binding proteins in vertebrates”, *Molecular and Cellular Biochemistry*, **239**, 69–77 (2002).

24. Haunerland, N. H., and F. Spener, “Fatty acid-binding proteins - Insights from genetic manipulations”, *Progress in Lipid Research*, **43**, 328–349 (2004).

25. Rodriguez-Calvo, R., J. Girona, J. M. Alegret, A. Bosquet, D. Ibarretxe, and L. Masana, “Role of the fatty acid binding protein 4 in heart failure and cardiovascular disease”, *J. Endocrinol.*, JOE-17-0031, (2017). doi:10.1530/JOE-17-0031

26. Liu, R.-Z., R. Mita, M. Beaulieu, Z. Gao, and R. Godbout, “Fatty acid binding proteins in brain development and disease”, *Int. J. Dev. Biol.*, **54**, 1229–39 (2010).

27. Zhang, W., R. Chen, T. Yang, N. Xu, J. Chen, Y. Gao, and R. A. Stetler, “Fatty acid transporting proteins: Roles in brain development, aging, and stroke”, *Prostaglandins Leukotrienes and Essential Fatty Acids*, (2017). doi:10.1016/j.plefa.2017.04.004

28. Paulussen, R. J. A., and J. H. Veerkamp, “Intracellular Fatty-Acid-Binding Proteins Characteristics and Function”, *Subcell. Biochem.*, **16**, 175-226 (1990).

29. Kumagai, A., R. Ando, H. Miyatake, P. Greimel, T. Kobayashi, Y. Hirabayashi, T. Shimogori, and A. Miyawaki, “A bilirubin-inducible fluorescent protein from eel muscle”, *Cell*, **153**, 1602–1611 (2013).

30. Iwatani, S., H. Nakamura, D. Kurokawa, K. Yamana, K. Nishida, S. Fukushima, T. Koda, N. Nishimura, H. Nishio, K. Iijima, A. Miyawaki, and I. Morioka, “Flourescent protein-based detection of unconjugated bilirubin in newborn serum”, *Sci. Rep.*, **6**, 28489, doi: 10.1038/srep28489 (2016).

31. Park, J.-S., E. Nam, H.-K. Lee, M. H. Lim, and H.-W. Rhee, “In Cellulo Mapping of Subcellular Localized Bilirubin” *ACS Chem. Biol.*, **11**, 2177–2185 (2016).

32. To, T., Q. Zhang, and X. Shu, “Structure- guided design of a reversible fluorogenic reporter of protein- protein interactions” *Protein Sci.*, **25**, 748–753 (2016).

33. Erapaneedi, R., V. V Belousov, M. Schäfers, and F. Kiefer, “A novel family of fluorescent hypoxia sensors reveal strong heterogeneity in tumor hypoxia at the cellular level” *EMBO J.*, **35**, 102–113 (2016).

34. Shitashima, Y., T. Shimozawa, T. Asahi, and A. Miyawaki, “A dual-ligand-modulable fluorescent protein based on UnaG and calmodulin”, *Biochem. Biophys. Res. Commun.*, **496**, 872-879 (2018).

35. Dean, K. M., and A. E. Palmer, “Advances in fluorescence labeling strategies for dynamic cellular imaging” *Nat. Chem. Biol.*, **10**, 512–523 (2014).

36. Plamont, M.-A. A., E. Billon-Denis, S. Maurin, C. Gauron, F. M. Pimenta, C. G. Specht, J. Shi, J. Quérard, B. Pan, J. Rossignol, N. Morellet, M. Volovitch, E. Lescop, Y. Chen, A. Triller, S. Vriz, T. Le Saux, L. Jullien, and A. Gautier, “Small fluorescence-activating and absorption-shifting tag for tunable protein imaging in vivo”, *Proc. Natl. Acad. Sci. U. S. A.*, **113**, 497–502 (2016).

37. Shimozawa, T., K. Yamagata, T. Kondo, S. Hayashi, A. Shitamukai, D. Konno, F. Matsuzaki, J. Takayama, S. Onami, H. Nakayama, Y. Kosugi, T.M. Watanabe, K. Fujita, and Y. Mimori-Kiyosue, “Improving spinning disk confocal microscopy by preventing pinhole cross-talk for intravital imaging”, *Proc. Natl. Acad. Sci . U. S. A.*, **110**, 3399–3404 (2013).

38. Baird, G. S., D. A. Zacharias, and R. Y. Tsien, “Biochemistry, mutagenesis, and oligomerization of DsRed, a red fluorescent protein from coral”, *Proc. Natl. Acad. Sci. U. S. A.*, **97**, 11984–11989 (2000).

39. Campbell, R. E., O. Tour, A. E. Palmer, P. A. Steinbach, G. S. Baird, D. A. Zacharias, and R. Y. Tsien, “A monomeric red fluorescent protein”, *Proc. Natl. Acad. Sci. U. S. A.*, **99**, 7877–7882 (2002).

Chapter 2

Two Fluorescence states of UnaG

2.1 Introduction

As described in Chapter 1, important molecular properties of UnaG for their use as FPs remain unknown although UnaG has a great potential as a fluorescent probe. These include the association/dissociation rate constants and their dispersion in aqueous solution. The purpose in this chapter is to investigate the physicochemical properties of UnaG. In 2013, UnaG was reported by Miyawaki group at RIKEN, and it has been utilized as fluorescent bilirubin determination method in serum. I thought that I would like to investigate the physicochemical properties of UnaG, and open the possibility for the UnaG applications. I determined the several fundamental features of UnaG such as the dispersibility, various rate constants, and fluorescent property from analytical ultracentrifugation analysis, spectroscopic analysis, and fluorescent intensity distribution analysis (FIDA) (Figure 2.1). The most remarkable achievement in this chapter is discovering the distinctive fluorescence intensity transition after addition of BR to apoUnaG solution while measuring the association/dissociation rates of UnaG and BR. I identified the unique fluorescent property of UnaG by the time-dependent green fluorescence of holoUnaG. Interestingly, after addition of BR to apoUnaG solution, the solution immediately showed strong fluorescence, and the intensity gradually increased to a plateau. Although distinctive photo activation fluorescent proteins were reported [1, 2], the fluorescent protein that gradually increased its FI after showing strong fluorescence has not been reported. I believed that clarifying the mechanism of this unique phenomenon was important for utilizing UnaG as a fluorescence probe [3]. By using these results, I suggested a novel schema of the UnaG

and BR complex system, and determined the various rate constants in the schema. Moreover, from analytical ultracentrifugation analysis, I also demonstrated that both apoUnaG and holoUnaG exist as monomers in aqueous solution even under conditions of 300 mM NaCl.

This part is reproduced with permission from Yoh Shitashima, Togo Shimozawa, Akiko Kumagai, Atsushi Miyawaki, and Toru Asahi, Two distinct fluorescence states of the ligand-induced green fluorescent protein UnaG, *Biophysical Journal*, 113, 2805-14 (2017) [4], Elsevier, copyright 2017. Consent from all authors has been secured.

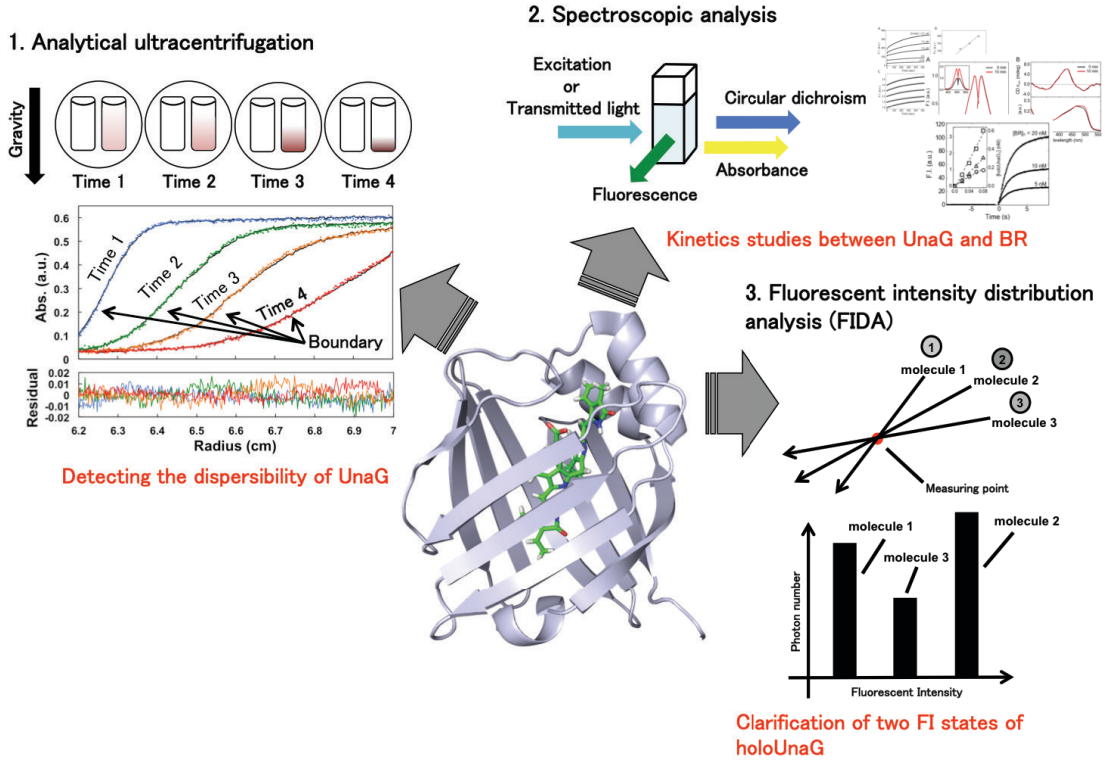

Figure 2.1. The approach for determination the fundamental study on UnaG. Some analyzing methods were used for determining the molecular properties of UnaG and finally a novel schema of the UnaG and BR complex system was suggested. The cartoon image of UnaG was created using PyMol (DeLano Scientific) from PDB files 4I3B [5].

2.2 Experimental Section

2.2.1 Chemicals

BR, dimethylsulfoxide (DMSO), and ampicillin sodium were purchased from Wako Pure Chemicals Industries, Ltd. (Osaka, Japan). Isopropyl-β-D-thiogalactopyranoside (IPTG) was purchased from Takara Bio Inc. (Shiga, Japan). Imidazole was purchased from Tokyo Chemical Industry Co., Ltd. (Tokyo, Japan). BR was dissolved in DMSO (1 mM) and stored at −20°C until use.

2.2.2 Preparation of Protein

The *UnaG* gene was provided by Kumagai A. and A. Miyawaki at RIKEN (Japan). The *UnaG* in the *pGEX-2T* vector was digested via *BamHI* and *EcoRI* restriction site, and was cloned into the *pColdI* (Takara Bio Inc., Shiga, Japan) vector. The plasmid encoding 6x His-tagged apoUnaG protein (pColdI-UnaG) was introduced into *E. coli. BL21* cells (Takara Bio Inc.). This transformed *E. coli.* cell was cultivated in LB medium (1% Bacto trypton, 0.5% Bacto yeast extract, 1% NaCl, ph7.0) supplemented with ampicillin (100 μg/mL) at 37^{o}C. After cultivation for 3 h, IPTG (0.5 μM) was added to the medium, and cultivation was continued for an additional 18 h at 16^{o}C. Cells were harvested by centrifugation, washed once with potassium phosphate buffer (20 mM, pH7.5, K-Pi buffer). Packed by centrifugation, cells were stored at −80°C until use. Packed cell were thawed and homogenized by sonication in K-Pi buffer for protein purification. The 6x His-tagged apoUnaG was purified from the soluble fractions of *E.coli.* by using HisTrap HP 1mL column (GE Healthcare UK, Ltd., Buckinghamshire, U.K.). The column bound to 6x His-tagged apoUnaG was washed with 10 mL wash buffer (pH 7.5) containing K-Pi (20 mM), NaCl (500 mM), and

imidazole (20 mM) before elution. 6x His-tagged apoUnaG was eluted with 2.5 mL elution buffer (pH 7.5) containing K-Pi (20 mM), NaCl (500 mM), and imidazole (500 mM), and desalted with a PD-10 column (GE Healthcare UK, Ltd.) equilibrated with K-Pi buffer containing Sodium azide (0.02%, vol/vol). The purified protein solution stored at 4^{o}C until use. Although the purified 6xHis-UnaG without digestion of the 6xHis-tag was used, I refer to 6xHis-UnaG as UnaG for simplification of the description in this study.

The plasmid for expression of UnaG N57A (Arg57 residue was replaced with Ala) [5], which showed faint fluorescence, was constructed by using the KOD -Plus-Mutagenesis kit (TOYOBO Co., Ltd., Osaka, Japan) according to the instruction manual. Mutations were introduced into the *UnaG* gene in *pColdI*, and correct generation of desired mutations was confirmed by DNA sequencing.

2.2.3 Analytical Ultracentrifugation

Sedimentation velocity experiments (AUC-SV) and sedimentation equilibrium experiments (AUC-SE) [6, 7] were performed on a Beckman Optima XL-I analytical ultracentrifuge at 20^{o}C. There experiments were performed to examine the sedimentation coefficient distribution (c(s)) and the molecular weight (MW) of UnaG, respectively. The density of buffer and partial specific volume (*Vp*) of 6 His-tagged UnaG were calculated using the SEDNTERP software (http://sednterp.unh.edu/), and were set as 1.002 g/ml and 0.74 cm^3/g, respectively. On AUC-SV, 400 μl of UnaG (15 μM, 0.8 absorbance unit (AU) at 280 nm) with BR (7.5 μM) in K-Pi buffer were loaded into two channel cells. Absorbance profiles, as a function of radius, were measured at 280 nm and 500 nm. The data were collected 50 times every 6 minutes at 55K rpm, and

analyzed by continuous c(s) distribution model using the SEDFIT software (Peter Shuck, NIH; http://www.analyticalultracentrifugation.com/). The c(s) ranging from 0.5 to 14.5 S were used for examination in wide-range, and 0.2–3 S were used for validation of peak shape with a resolution of 200 in both ranges. On s AUC-SE, 100 μl of UnaG at 9.4 μM, 5.6 μM, and 3.8 μM (0.5, 0.3, and 0.2 absorbance unit, respectively) for apoUnaG and 1:1 mixture of UnaG and BR at same concentrations for holoUnaG were loaded into six channel cells. The data were analyzed globally at 25K rpm by nonlinear least-squares analysis using the ORIGIN software package supplied by Beckman.

2.2.4 Spectroscopic Studies

Spectroscopic analysis for excitation and fluorescence spectra and FI time-course of holoUnaG were performed using a RF-5300PC spectrometer (Shimadzu Corporation, Kyoto, Japan). In all experiment, the excitation wavelength and emission wavelength were set at 490 nm and 525 nm, respectively, and both bandwidths were set at 5 nm. Circular Dichroism (CD) and absorption spectra were recorded using a J-820 Spectropolarimeter (JASCO Corporation, Tokyo, Japan). 2 ml of samples containing apoUnaG, BR, DMSO (at most 0.2%, vol/vol), and K-Pi buffer were loaded into the quartz cuvette having a path length of 1 cm. All data were collected at room temperature.

2.2.5 Fluorescence intensity distribution analysis (FIDA)

Fluorescence intensity distribution analysis (FIDA) [8, 9] was performed using an MF20 apparatus (Olympus Corporation, Tokyo, Japan) with a confocal microscope and laser. I used the adjustment Dye Kit 488 nm (MF-D488PX-2) as a control measurement.

I measured 50 μl of sample contained apoUnaG (100 nM), BR (10 nM), DMSO (1%, vol/vol) in K-Pi buffer (20 mM, pH7.5), and control sample (adjustment Dye Kit 488 nm, MF-D488PX-2, Olympus Corporation) in glass-bottom 384-well dishes. The sample solution was excited by the 100 μW of 488 nm Ar-laser with beam scanner at 3,600 rpm, and data was measured automatically at a dwell time of 40 μs at each monitoring (a total measuring time was 10 s per sample). The data was analyzed automatically using software installed in MF20 system. All data were collected at room temperature.

2.3 Results

2.3.1 FI Increase in two phases after mixing of UnaG and BR

I first attempted to measure the association rate of UnaG and BR by analyzing the kinetics of the FI time-course spectrophotometrically after mixing UnaG and BR. However, in the process of the evaluation, I found the unique fluorescent property of holoUnaG. The FI time-course did not agree with the conventional model assuming a simple fluorescent complex formation by binding BR. To confirm the fluorescence intensity (FI) transition after adding BR to apoUnaG, I examined the FI time courses after adding BR to various concentrations of apoUnaG solution (Figure 2.2A). The time-dependent green fluorescence of apoUnaG upon addition of BR indicated that the brightness of holoUnaG exhibited two phases; an immediate rapid phase followed by a slow phase. The rapid phase would be due to the BR engagement within apoUnaG, because (i) the complex formation is the primary event after mixing of UnaG and BR, and (ii) the amplitudes of each rapid phase (FI_0) increased in proportion to the holoUnaG concentration unambiguously, which is equivalent to the amount of generated holoUnaG (Figure 2.2B). In addition, the association of apoUnaG and BR would be to proceed rapidly because of the high affinity of UnaG and BR (K_d = 98 pM) [5]. On the other hand, the FI time course in slow phase, normalized by each FI_0, seemed to show the same exponential curve (Figure 2.2C). The fitting analysis of each curve was achieved by using the following Equation (2.1) as fitting function:

$$FI_{nor}(t) = A\left(1 - e^{-kt}\right) + 1 \quad \cdots \text{Equation (2.1)}$$

where FI_{nor} (t), A and k were the FI at time t, amplitude, and the rate constant, respectively. The result in five apoUnaG concentrations suggested the same rate

constant and amplitude (k = 4.34 × 10^{-3} ± 0.18 s^{-1} and A = 0.78 ± 0.02; Figure 2.2D). The simple exponential kinetics of the slow phase, without dependence on the concentrations of holoUnaG and free BR, indicated that the FI transition in slow phase was not caused by protein-protein association such as holoUnaG itself, and holoUnaG and apoUnaG.

Furthermore, I examined the sequential BR adding experiments in 1 μM apoUnaG solution to ascertain whether the abundance of apoUnaG induced this reaction. I added BR four times every 5 minutes to apoUnaG liquid solution, and BR concentrations were adjusted to 0 μM, 0.25 μM, 0.5 μM, 0.75 μM and 1 μM, respectively (Figure 2.3A). The FI_0 after first BR addition was as same as the FI_0 after fourth BR addition (Figure 2.3B), supporting that FI transition in second phase is not caused by the interaction between apoUnaG and holoUnaG.

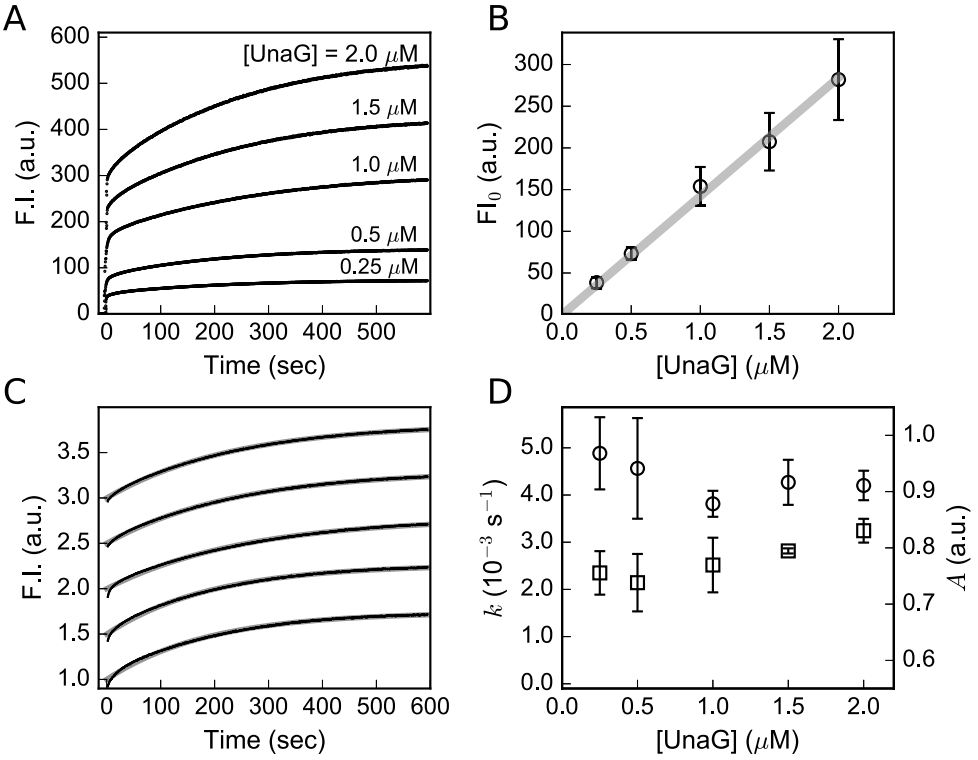

Figure 2.2. Two distinct rates in the FI time-courses upon the mixing of UnaG and BR. (A) The FI time-courses after mixing UnaG and BR. BR was added to apoUnaG solution (BR:UnaG = 1:1) at various concentrations (in ascending order: 0.25, 0.5, 1.0, 1.5, 2.0 μM in final concentration) at 0 sec. (B) The plot of the FI amplitudes increases in the rapid phase (FI_0) vs. the UnaG concentrations in the solution. (C) Normalized FI time-courses in the slow phase displayed in (A) (black dots) with fitting curves achieved by using Equation (2.1) (gray line). The time-courses were normalized by respective FI_0 and were presented with each 0.5 increment on the vertical axis for visibility. (D) The plot of the time constants and the amplitudes of FI enhancement obtained from the fitting analysis in (C). The time constants (open circles, left axis) and the amplitudes (open squares, right axis) had no dependence on the UnaG concentrations and were determined to be $k = 4.34 \times 10^{-3} \pm 0.18\ s^{-1}$ and A = 0.78 ± 0.02 on average. Each curve presents in (A) and (C) is a typical curve selected from four independent experiments at each UnaG concentration. Data are averages from four independent experiments, and error bars indicate standard deviations in (B) and (D). Reprinted with permission from Yoh Shitashima, Togo Shimozawa, Akiko Kumagai, Atsushi Miyawaki, and Toru Asahi, Two distinct fluorescence states of the ligand-induced green fluorescent protein UnaG, *Biophysical Journal*, 113, 2805-2814 (2017) [4], Elsevier, copyright 2017. Consent from all authors has been secured.

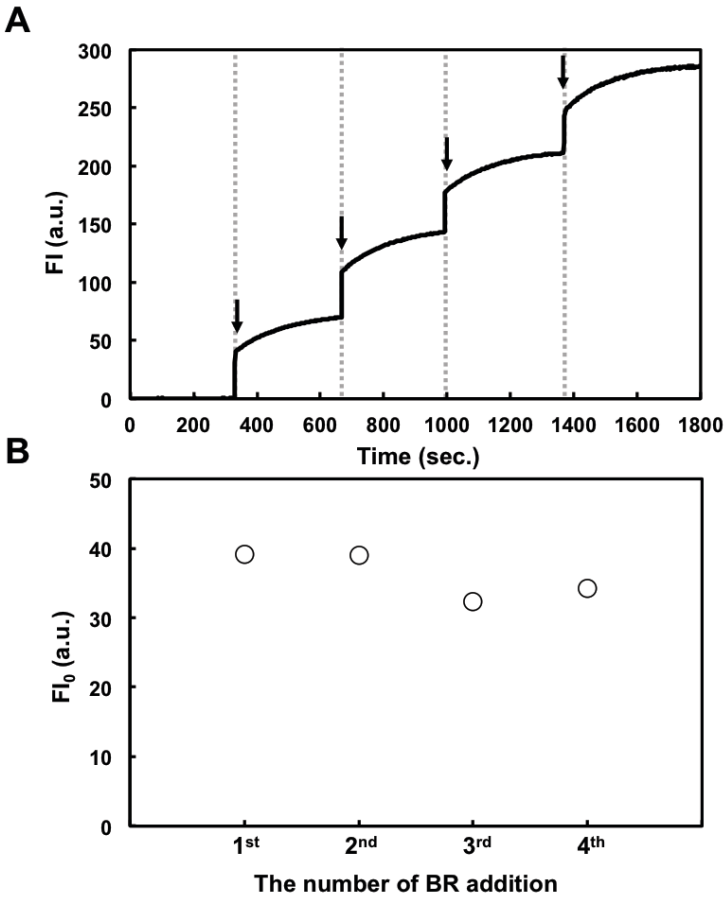

Figure 2.3. Sequential BR adding experiments in 1 mM purified apoUnaG solution. (A) Same amount of BR were added four times every 5 minutes (the arrows show the BR adding time), and BR concentrations were adjusted to 0 μM, 0.25 μM, 0.5 μM, 0.75 μM and 1 μM, respectively. Immediately increased FI phase (fast phase) was completely separated from gradually increased FI phase (slow phase). (B) The initial FI (FI_0) after first, second, third and fourth BR addition.

2.3.2 The non-relationship between slow phase and protein dissociation

The kinetic analyses in Figure 2.2 did not prove the information of involvement of holoUnaG dissociation assemblies in the slow FI increase. Therefore, I subjected UnaG to analytical ultracentrifugation in order to investigate this possibility. I first used the AUC-SV to examine the sediment coefficient distribution (c(s)) of an equimolar mixture of apoUnaG and holoUnaG (7.5 μM each) in the same buffer as for the data presented in Figure 2.2. Figure 2.4A shows the absorbance profiles measured at 280 nm, where both apoUnaG and holoUnaG were detected, with fitting curves by SEDFIT using c(s) as parameters. The c(s) distribution obtained from the absorbance profiles showed only one symmetrical peak (Figure 2.4B), and this result indicated that both apoUnaG and holoUnaG exhibit same sedimentation coefficients (~1.8 S). I also measured at a wavelength of 500 nm to determine the sedimentation coefficient of holoUnaG, because holoUnaG has the additional maximum absorption around 500 nm due to the absorbance of bound BR whereas apoUnaG has only maximum absorption around 280 nm. The sedimentation coefficient of holoUnaG has almost the same c(s) (Figure 2.5), supporting the identical sedimentation coefficients of apoUnaG and holoUnaG. Additionally, the almost same c(s) was obtained under the conditions of high NaCl concentration (300 mM) (Figure 2.6). Together with the sedimentation coefficients of ~1.8 S and the primary structure of UnaG (140 amino-acid including 6xHis-tag and linker), it is suggested that both apoUnaG and holoUnaG exist as monomers in K-Pi buffer. These results show that the slow FI increase was also not caused by dissociation of holoUnaG assemblies.

I also used the AUC-SE to determine the dispersion of monomers by directly determining the molecular weights (MWs) of apoUnaG and holoUnaG. The absorbance

profiles of apoUnaG (Figure 2.4C) and holoUnaG (Figure 2.4D) in sedimentation equilibrium (after centrifugation for 16 h) obtained from the global curve fitting of three different data and the residuals of the fittings (bottoms in Figure 2.4C and D) are shown. The fitted molecular weight of apoUnaG and holoUnaG were estimated to be 20,928 Da and 21,299 Da, respectively. These experimental MWs were similar to the MWs calculated from the primary structures of apoUnaG (including 6xHis-tag and linker; 18,651 Da) and holoUnaG (same as above; 19,236 Da). These results indicated that both apoUnaG and holoUnaG were monomers in K-Pi buffer.

The kinetic analyses (Figure 2.2) and the monomeric dispersion of both apoUnaG and holoUnaG (Figure 2.4) indicated that the slow FI increase was associated with an intra-molecular reaction within the already formed holoUnaG molecule. These results suggested that holoUnaG exists in two states with different fluorescence intensities, which were named holoUnaG$_1$ and holoUnaG$_2$. The holoUnaG$_1$ molecule initially forms after binding BR, and then changes to the brighter holoUnaG$_2$ molecule by this intra-molecular reaction.

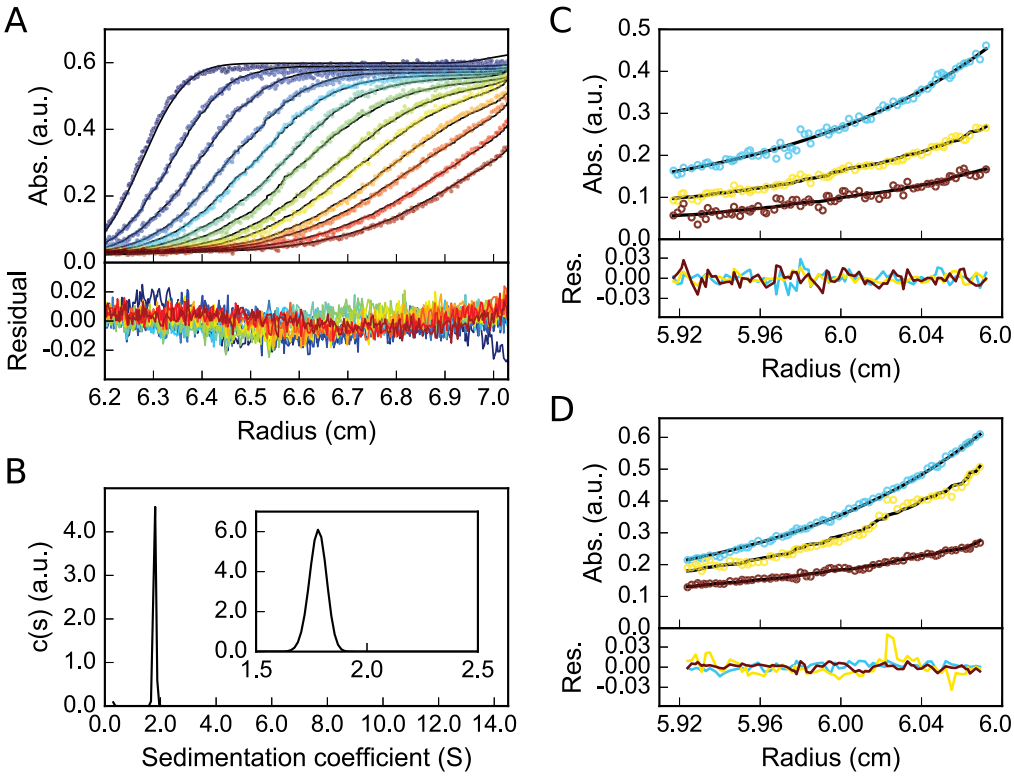

Figure 2.4. Analytical ultracentrifugation of apoUnaG and/or holoUnaG. (A) (Top) Sedimentation velocity absorbance profiles of an equimolar mixture of apoUnaG and holoUnaG (7.5 μM each) in K-Pi buffer (colored dots, higher color temperature indicate later time points) with fitting curves (black lines), using c(s) as parameters by SEDFIT software. (Bottom) Residuals of the fittings are shown in the bottom panel. The absorbance profiles were obtained at 55K rpm and 20°C, and were collected every 6 min for 300 min. Scans presented here are every 24 min for clarity. The fitting analysis was performed with a grid resolution of 200 for 0.5–15 S. (B) The c(s) as a result of the fitting analysis in graph (A). (inset) The detailed c(s) obtained by limiting the range of c(s) to 1.0–2.5 S with grid resolution of 200. Both c(s) showed a single peak without a shoulder. (C and D) (Tops) Sedimentation equilibrium absorbance profiles for various concentrations of apoUnaG (C) and holoUnaG (D) (colored circles, blue: 9.4 μM; yellow: 5.6 μM; and red: 3.8 μM), and the fitting curves (black lines) that are analyzed globally by a nonlinear least-squares method. (Bottoms) Residuals of the fittings are shown in the bottom panel. The absorbance profiles were obtained at 25K rpm and 20°C. Reprinted with permission from Yoh Shitashima, Togo Shimozawa, Akiko Kumagai, Atsushi Miyawaki, and Toru Asahi, Two distinct fluorescence states of the ligand-induced green fluorescent protein UnaG, *Biophysical Journal*, 113, 2805-2814 (2017) [4], Elsevier, copyright 2017. Consent from all authors has been secured.

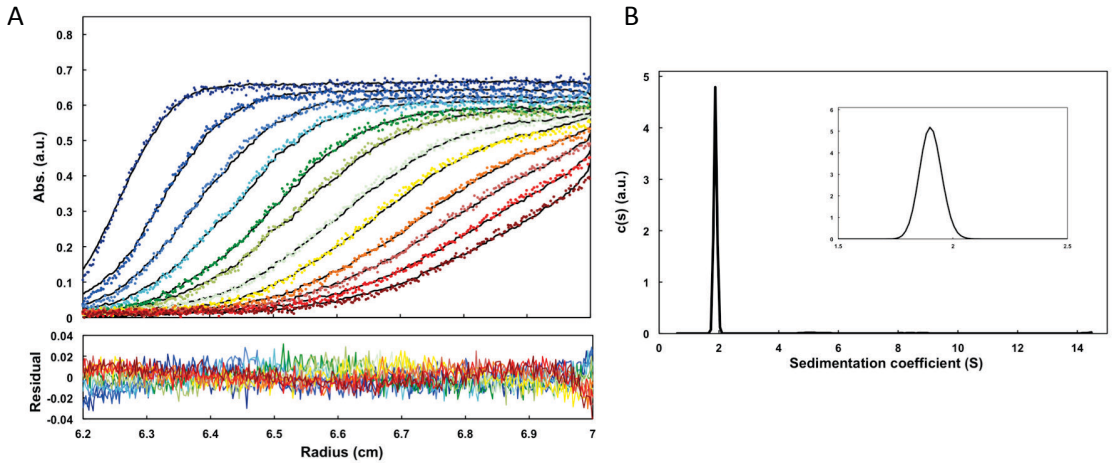

Figure 2.5. Sedimentation velocity analysis of apoUnaG and holoUnaG mixture measured at 500 nm. (A) Sedimentation velocity absorbance profiles, and (B) the c(s) as a result of the fitting analysis in graph (A). HoloUnaG has a sedimentation coefficient of ~1.8 S. Reprinted with permission from Yoh Shitashima, Togo Shimozawa, Akiko Kumagai, Atsushi Miyawaki, and Toru Asahi, Two distinct fluorescence states of the ligand-induced green fluorescent protein UnaG, *Biophysical Journal*, 113, 2805-2814 (2017) [4], Elsevier, copyright 2017. Consent from all authors has been secured.

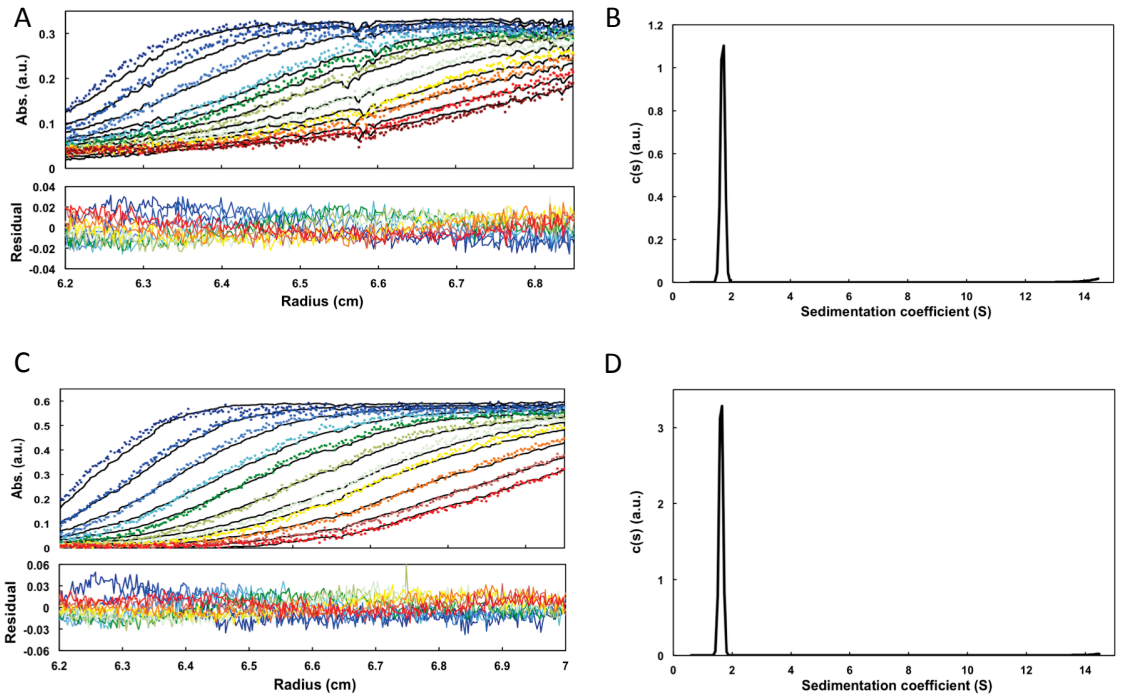

Figure 2.6. Sedimentation velocity analysis of apoUnaG and holoUnaG mixture in the presence of 300 mM NaCl. (A) Sedimentation velocity absorbance profiles, and (B) the c(s) as a result of the fitting analysis in graph (A) measured at 280 nm. (C) Sedimentation velocity absorbance profiles, and (D) the c(s) as a result of the fitting analysis in graph (C) measured at 500 nm. Both c(s) showed a single peak without a shoulder. Both apoUnaG and holoUnaG have the same sedimentation coefficients of ~1.8 S at high salt concentration. Reprinted with permission from Yoh Shitashima, Togo Shimozawa, Akiko Kumagai, Atsushi Miyawaki, and Toru Asahi, Two distinct fluorescence states of the ligand-induced green fluorescent protein UnaG, *Biophysical Journal*, 113, 2805-2814 (2017) [4], Elsevier, copyright 2017. Consent from all authors has been secured.

2.3.3 The two distinct fluorescence states of holoUnaG

In order to confirm the presence of the two states of holoUnaG, I utilized the fluorescence-intensity distribution analysis (FIDA) to examine the distribution and molecular brightness ratio of holoUnaG$_1$ and holoUnaG$_2$ at the plateau of the slow phase. The summarized results of FIDA for Rhodamine-110, the standard solution, and holoUnaG solution at steady state were given in Table 2.1. The result from the Rhodamine-110 solution was well fitted by single component analysis, while the holoUnaG solution showed good agreement with the two-component model showing a population ratio of 60:40 and molecular brightness ratio of 1:3.9 for holoUnaG$_1$:holoUnaG$_2$. This co-existence of holoUnaG$_1$ and holoUnaG$_2$ at plateau of the slow phase demonstrates the presence of the two states of holoUnaG and the reversibility of the intra-molecular reaction, and finally reaching equilibrium between two states.

Figure 2.7 shows the details of the UnaG and BR complex system to provide its overall schema more clearly. The apoUnaG binds to BR and forms the holoUnaG$_1$, and finally changes to the brighter holoUnaG$_2$ by a reversible intra-molecular reaction (k_{12}, k_{21}). The BR dissociation pathways for holoUnaG$_1$ and holoUnaG$_2$ (holoUnaGs) were shown in dashed arrows because the results obtained in this study indicated that: (i) at least either k_{off1} or k_{off2}, were not 0, and (ii) the unique values of k_{off1} and k_{off2} could not be determined (as described below). If I had obtained the transient dynamics of the distribution of the two states during the slow phase, I could have suggested the reaction model more clearly. Note, however, that FIDA can be performed only at the steady state because the calibration requires at least ~5 min.

Table 2.1. Results of fluorescence intensity distributions analysis

Sample	q_1 (kHz)	q_2 (kHz)	C_1 (%)	C_2 (%)	χ^2
Rhodamine-110	60.5±0.4	-	100	-	1.0
holoUnaG	11.5±2.1	44.9±1.3	60.3±1.6	39.7±1.6	1.5

The results from Rhodamine-110 and holoUnaG were fitted by single and two component(s) analysis, respectively. The variables q_1 and q_2 are the photon count rates of the components, i.e., the brightness of respective molecular species. The C_1 and C_2 are the distributions of respective molecular species. In all cases, the background photon count rate was fixed to 0.74 kHz, as measured with K-Pi buffer. Data were averaged from ten independent experiments, and error indicates standard deviations of the mean. Reprinted with permission from Yoh Shitashima, Togo Shimozawa, Akiko Kumagai, Atsushi Miyawaki, and Toru Asahi, Two distinct fluorescence states of the ligand-induced green fluorescent protein UnaG, *Biophysical Journal*, 113, 2805-2814 (2017) [4], Elsevier, copyright 2017. Consent from all authors has been secured.

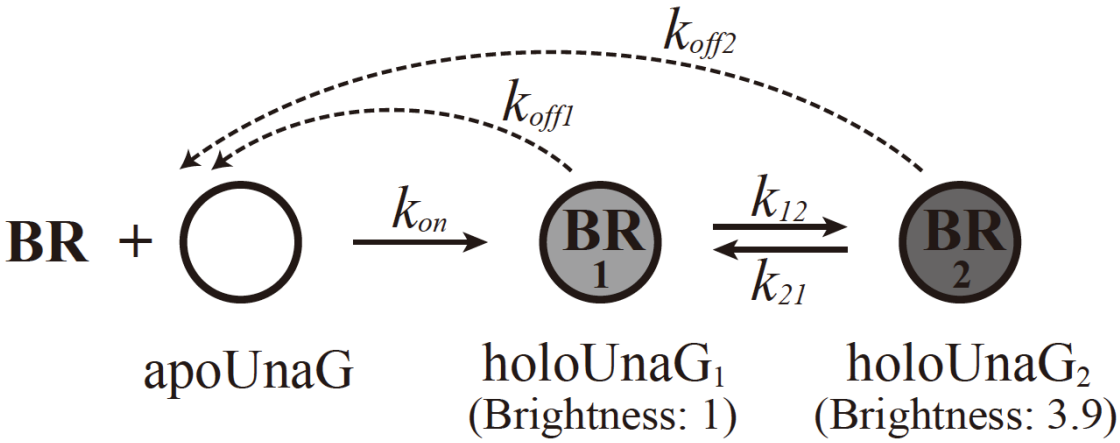

Figure 2.7. Proposed schema of the UnaG and BR complex system. The holoUnaG$_1$ was initially formed by the binding of apoUnaG and BR. Then, by a reversible intra-molecular reaction, holoUnaG$_1$ changed to holoUnaG$_2$ and brightness increased by a factor of 3.9x. The apoUnaG, holoUnaG$_1$, and holoUnaG$_2$ finally reached a state of equilibrium. The BR dissociation pathways for holoUnaG$_1$ and holoUnaG$_2$ are indicated by dashed arrows because: (i) at least either k_{off1} or k_{off2} was not 0; (ii) the unique values of k_{off1} and k_{off2} could not be determined (for details, see main text). Reprinted with permission from Yoh Shitashima, Togo Shimozawa, Akiko Kumagai, Atsushi Miyawaki, and Toru Asahi, Two distinct fluorescence states of the ligand-induced green fluorescent protein UnaG, *Biophysical Journal*, 113, 2805-2814 (2017) [4], Elsevier, copyright 2017. Consent from all authors has been secured.

2.3.4 Spectroscopic studies for investigation of the change in BR

To confirm the difference of BR fluorophore between holoUnaG$_1$ and holoUnaG$_2$, the excitation, emission, circular dichroism (CD) and absorption spectra of the solution at the start and the plateau of the slow phase (at 0 and 10 min from the start of the slow phase) was measured (Figure 2.8). In case of the excitation and fluorescence spectra, the intensity increased ~1.7-fold (Figure 2.8A, inset) with the same spectral shapes, indicating that the intra-molecular reaction enhanced the fluorescent efficiency of BR without change of the chemical structure. Similarly, both intensity and spectral shape of the CD and absorption spectra did not change (Figure 2.8B, upper, CD; lower, absorption), suggesting that the intra-molecular reaction did not affect the chemical structure change or the conformational change of BR. This result also suggested that no additional BR bound to UnaG during the slow phase. Moreover, no changes in the CD spectra around UV range indicated that the intra-molecule reaction did not affect the secondary structure of UnaG (Figure 2.9).

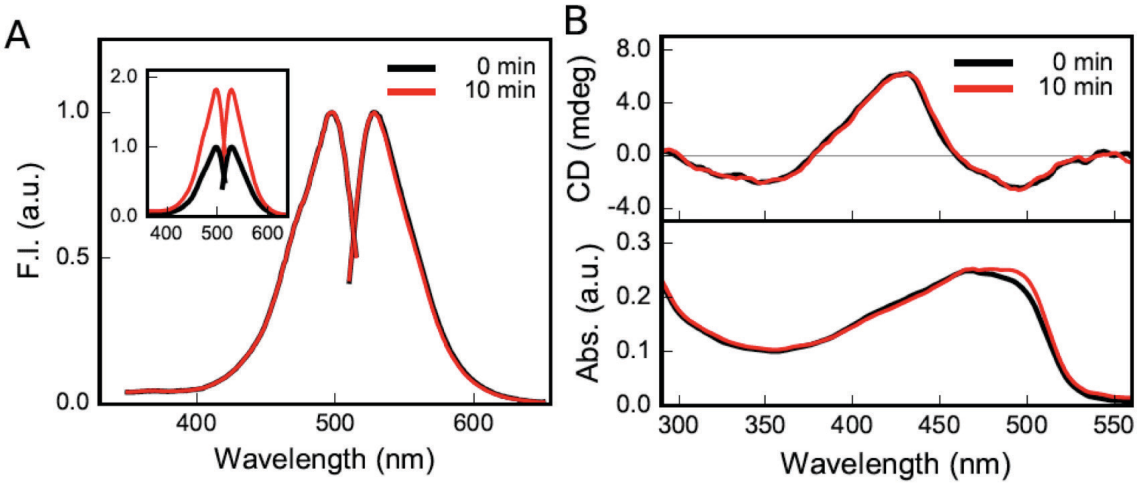

Figure 2.8. Spectroscopic studies to probe the change in bound BR. (A) The excitation and fluorescence spectra of 1 μM holoUnaG (both UnaG and BR, 1 μM) at 0 and 10 min from the start of the slow phase (black and red lines, respectively). Each spectrum was normalized by its own FI maximum. (inset) The spectra normalized by the FI maxima at 0 min (B) The CD (top) and absorption (bottom) spectra of 1 μM holoUnaG were presented in corresponding colors to (A) (UnaG and BR, 1 μM and 5 μM; The condition was set for excess BR in solution to prevent BR dissociation for measurements over a long time period). Reprinted with permission from Yoh Shitashima, Togo Shimozawa, Akiko Kumagai, Atsushi Miyawaki, and Toru Asahi, Two distinct fluorescence states of the ligand-induced green fluorescent protein UnaG, *Biophysical Journal*, 113, 2805-2814 (2017) [4], Elsevier, copyright 2017. Consent from all authors has been secured.

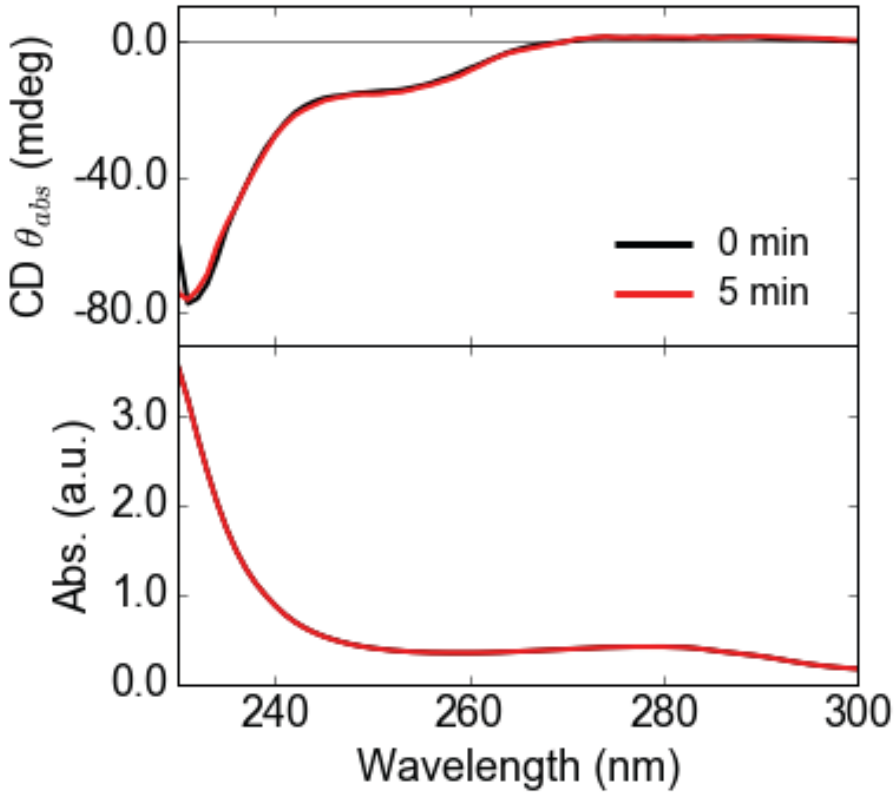

Figure 2.9. CD and absorption spectra of holoUnaG in UV region at 0 and 5 min from the start of the slow phase (both UnaG and BR, 7.5 μM). Reprinted with permission from Yoh Shitashima, Togo Shimozawa, Akiko Kumagai, Atsushi Miyawaki, and Toru Asahi, Two distinct fluorescence states of the ligand-induced green fluorescent protein UnaG, *Biophysical Journal*, 113, 2805-2814 (2017) [4], Elsevier, copyright 2017. Consent from all authors has been secured.

2.3.5 Analysis of transition rates between holoUnaG$_1$ and holoUnaG$_2$

By analyzing the normalized FI time-course of the slow phase, I estimated the individual values of k_{12} and k_{21}. By solving differential equations for the schema (Figure 2.7), the function was obtained (Equation (2.2)). The derivation of the function was described below. I set the condition as follows; (i) the population of holoUnaG$_1$ was 100% at t = 0, (ii) apoUnaG did not exist in the solution since the high affinity of UnaG and BR.

$$FI_{nor}(t) = (\alpha - 1) \cdot \frac{k_{12}}{k_{12} + k_{21}} \cdot \left(1 - e^{-(k_{12}+k_{21})\cdot t}\right) + 1 \quad \cdots \text{Equation (2.2)}$$

where α indicates the brightness ratio of holoUnaG$_2$ to holoUnaG$_1$, and equals to 3.9, as obtained by the FIDA (Table 2.1). The time constant in the function (k_{12} + k_{21}) correspond to the apparent transition rate of the slow phase in Figure 2.2D (k = 4.34 × 10^{-3} s^{-1}), and the ratio 1/k_{12}:1/k_{21} should correspond to the molecular distribution of 60:40 with the two states at steady state (Table 2.1). The k_{12} and k_{21} satisfying the two restrictions are determined to be 1.72 × 10^{-3} s^{-1} and 2.62 × 10^{-3} s^{-1}, respectively.

The derivation of the Equation (2.2)

The differential equations for the concentrations of holoUnaG$_1$ and holoUnaG$_2$ for the schema in Figure 2.7 were described as

$$\frac{d}{dt}\left[holoUnaG_1\right] = k_{on}\left[BR\right]\left[apoUnaG\right] - \left(k_{12} + k_{off1}\right)\left[holoUnaG_1\right] + k_{21}\left[holoUnaG_2\right]$$

$$\frac{d}{dt}\left[holoUnaG_2\right] = k_{12}\left[holoUnaG_1\right] - \left(k_{21} + k_{off2}\right)\left[holoUnaG_2\right]$$

Now I consider the situation of the slow phase of the FI increase. The boundary conditions were set to (i) all UnaG molecules were in holoUnaG$_1$ at t=0 ([holoUnaG$_1$]$_0$ = 1), (ii) the dissociation of BR was negligible due to the high affinity of UnaG and BR (k_{off1}, k_{off2}, [BR] and [apoUnaG] equal to zero). By some deformations of the formulas and solving the differential equations, I obtain,

$$\left[holoUnaG_1\right] = \frac{1}{k_{12} + k_{21}}\left(k_{21} + k_{12} \cdot e^{-(k_{12}+k_{21})t}\right)$$

$$\left[holoUnaG_2\right] = \frac{1}{k_{12} + k_{21}}\left(k_{12} + k_{12} \cdot e^{-(k_{12}+k_{21})t}\right)$$

The brightness of holoUnaG$_1$ and holoUnaG$_2$ were expressed as 1 and ✔, respectively, the normalized FI time-courses was represented by

$$FI_{nor}(t) = \left[holoUnaG_1\right] + \alpha\left[holoUnaG_2\right] = \left(\alpha - 1\right) \cdot \frac{k_{12}}{k_{12} + k_{21}} \cdot \left(1 - e^{-(k_{12}+k_{21})t}\right) + 1$$

2.3.6 The association rate constant of UnaG and BR

The association rate (k_{on}) of UnaG and BR was determined by analyzing the initial velocity of the FI increase in rapid phase. I set the total concentration of BR ($[BR]_0$) and UnaG ($[apoUnaG]_0$) within 50 nM in final concentration, and measured the FI time-courses upon mixing (Figure 2.10). Herein, the FI time-courses do not exhibit a simple exponential curve due to the FI enhancement in the slow phase, as described in Figure 2.2. Then, I focused on very initial part of the rapid phase, because the production of holoUnaG$_2$ and the resulting FI enhancement were negligible (Figure 2.10A, inset). For determination of the absolute value of k_{on}, the right axis of the inset figure shows the holoUnaG$_1$ concentration. For this conversion, I used the relationship that the FI_0 for 1 nM holoUnaG$_1$ equals to 5.60, which was measured in same manner as Figure 2.2 with the identical spectrophotometer setup in Figure 2.10A. The plot of the initial velocities of holoUnaG$_1$ generation (V_{init}) vs. $[BR]_0$ was shown in Figure 2.10B. Using the result of linear regression of this plot and the relationship of $V_{init} = k_{on} \cdot [apoUnaG]_0 \cdot [BR]_0$, the associated rate constant was determined to be $k_{on} = 7.05 \times 10^6\ M^{-1}s^{-1}$.

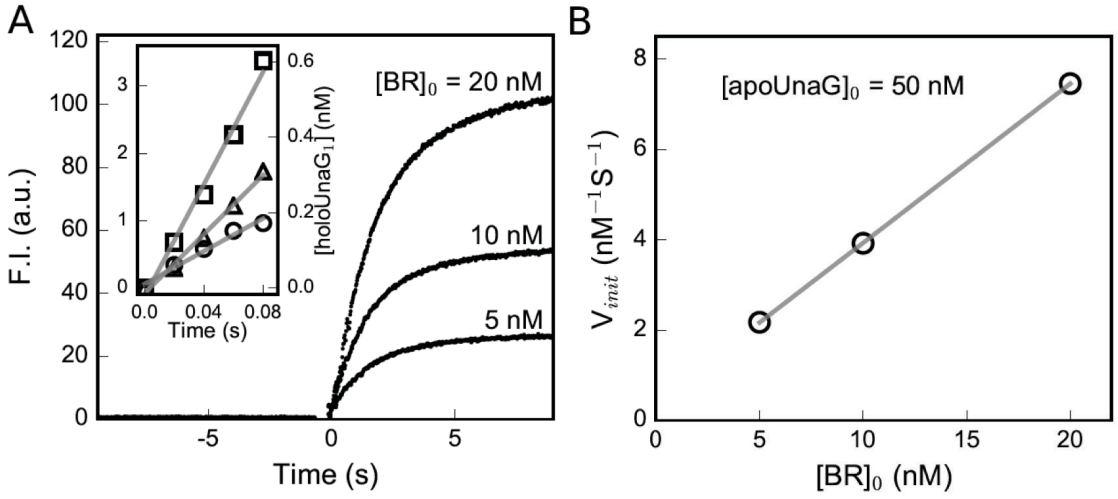

Figure 2.10. The association rate constant of UnaG and BR. (A) The FI time-courses upon addition of various concentrations of BR (5, 10 and 20 nM in final conc.) to apoUnaG solutions (50 nM, fixed). The total concentration of BR and UnaG in final concentration were denoted by $[BR]_0$ and $[apoUnaG]_0$, respectively. (A, inset) The FI time-courses focused on the very initial phase and the fitting lines were shown (in order from the bottom, $[BR]_0$ = 5, 10 and 20 nM). The right axis shows the concentration of $holoUnaG_1$corresponding to the raw FI value. The method to convert the raw FI value to $holoUnaG_1$ concentration is described in main text. (B) The plot of the initial velocities of $holoUnaG_1$ generation (V_{init}) vs. $[BR]_0$ (open circles) and the linear regression line (dashed gray line). The association rate constant (k_{on}) was obtained from the slope of this plot (k_{on} = 7.05 × 10^6 $M^{-1}s^{-1}$). Reprinted with permission from Yoh Shitashima, Togo Shimozawa, Akiko Kumagai, Atsushi Miyawaki, and Toru Asahi, Two distinct fluorescence states of the ligand-induced green fluorescent protein UnaG, *Biophysical Journal*, 113, 2805-2814 (2017) [4], Elsevier, copyright 2017. Consent from all authors has been secured.

2.3.7 The dissociation rate constant of UnaG and BR

In order to measure the apparent dissociation rate from holoUnaGs (k_{off}), I utilized the weak-fluorescent UnaG N57A mutant [5], which brightness was approximately 3% compared to wild-type (WT) UnaG, as an adsorbent of the free BR dissociated from holoUnaGs. First, I validated that the N57A mutant had a high affinity for BR, comparable to that of WT UnaG, from the fact that the FI of an equimolar mixture of WT holoUnaG and holo N57A mutant (1 μM each) without free BR at equilibrium state decreased by half compared to the FI of 1 μM WT holoUnaG (Figure 2.12). Figure 2.11 showed that exponential FI decay was induced by the addition of a large excess of N57A (~80x molar ratio) to WT holoUnaG solution at 0 min. Because the high concentration of N57A quickly depleted, the free BR dissociated from the WT holoUnaG in the solution. The time constant observed in the FI decay corresponded to the apparent dissociation rate of BR from the WT holoUnaG ($k_{off} = 2.17 \times 10^{-4}$ s^{-1}). The affinity calculated from k_{off}/k_{on} was K_d = 31 pM and was in good agreement with the reported affinity (K_d = 98 pM)[5], supporting the validity of our measurement of the two rates.

The unique values of k_{off1} and k_{off2} could not be determined because it was impossible to distinguish between the individual BR dissociations from holoUnaG$_1$ and holoUnaG$_2$. However, the relationship k_{off}, k_{off1} and k_{off2} was obtained by solving the differential equations under the condition that the concentration of free BR is negligible (Equation (2.3)). The derivation of the function was described below.

$$k_{off} = \frac{\left(-A + \sqrt{A^2 - 4B}\right)}{2} \quad \cdots \text{Equation (2.3)}$$

where the A and B mean,

$$A = k_{12} + k_{21} + k_{off1} + k_{off2}$$

$$B = k_{12} \cdot k_{off1} + k_{12} \cdot k_{off2} + k_{off1} \cdot k_{off2}$$

The k_{off1} and k_{off2} are 0 or positive values that satisfy Equation (2.3). Figure 2.13 shows the line expressing the possible set of (k_{off1}, k_{off2}), using the parameters obtained in this study ($k_{off} = 2.17 \times 10^{-4}$ s^{-1}, $k_{12} = 1.72 \times 10^{-3}$ s^{-1} and $k_{21} = 2.62 \times 10^{-3}$ s^{-1}).

The derivation of the Equation (2.3)

The differential equations for the concentrations of holoUnaG$_1$ and holoUnaG$_2$ for the schema in Figure 2.7 were already described above. Now I consider the situation that large excess amount of N57A mutants were added to the WT holoUnaG solution at the equilibrium of holoUnaG$_1$ and holoUnaG$_2$ at t = 0. In this situation, the free BR can be ignored because of the quick depletion by N57A mutants. By some algebraic manipulation and solving the differential equations, I obtain

$$\left[holoUnaG_1\right] = C_1 e^{\left(\frac{-A+\sqrt{A^2-4B}}{2}\right)\cdot t}$$

$$\left[holoUnaG_2\right] = C_2 e^{\left(\frac{-A+\sqrt{A^2-4B}}{2}\right)\cdot t}$$

where the A and B mean

$$A = k_{12} + k_{21} + k_{off1} + k_{off2}$$

$$B = k_{12}\cdot k_{off1} + k_{12}\cdot k_{off2} + k_{off1}\cdot k_{off2}$$

and the C_1 and C_2 can be determined from the boundary conditions, i.e., the initial concentrations of holoUnaG$_1$ and holoUnaG$_2$, as follows

$$C_1 = \frac{k_{12}}{k_{12}+k_{21}}\cdot\left[UnaG_0\right]$$

$$C_2 = \frac{k_{21}}{k_{12}+k_{21}}\cdot\left[UnaG_0\right]$$

where the [$UnaG_0$] mean the total concentration of UnaG proteins in the solution.

The apparent dissociation rate (k_{off}) correspond to the time constant in the formulas above, therefore, I finally obtain

$$k_{off} = \frac{\left(-A+\sqrt{A^2-4B}\right)}{2}$$

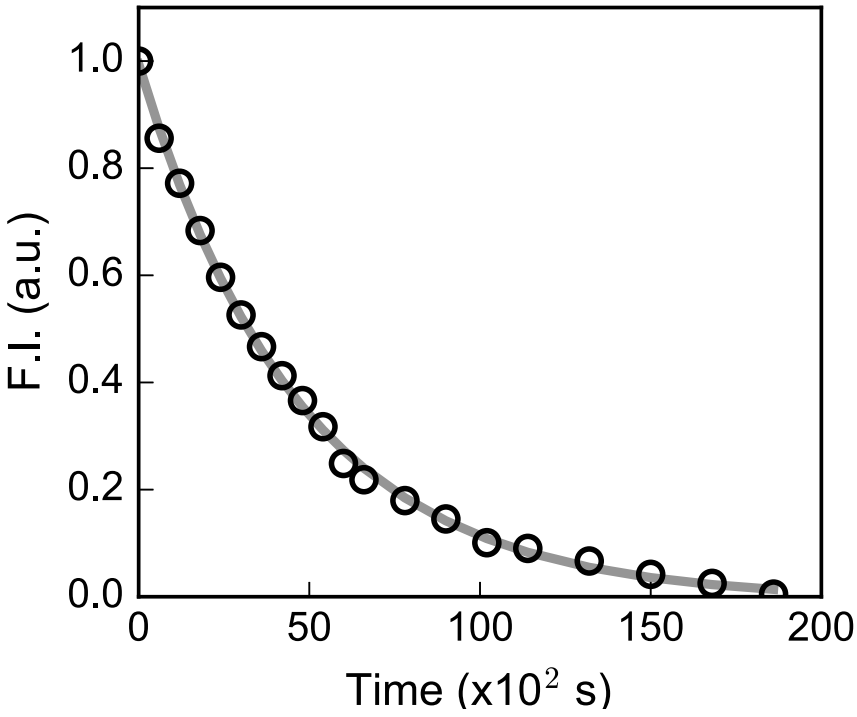

Figure 2.11. The dissociation rate constants of UnaG and BR. The FI time-course upon addition of 80x excess N57A (weak-fluorescent mutant) apoUnaG to the WT holoUnaGs solution at equilibrium state (opened circles) and fitting curve (gray line). The FI decay was well-fitted with a single exponential function with the time constant of 2.17×10^{-4} s^{-1}. Reprinted with permission from Yoh Shitashima, Togo Shimozawa, Akiko Kumagai, Atsushi Miyawaki, and Toru Asahi, Two distinct fluorescence states of the ligand-induced green fluorescent protein UnaG, *Biophysical Journal*, 113, 2805-2814 (2017) [4], Elsevier, copyright 2017. Consent from all authors has been secured.

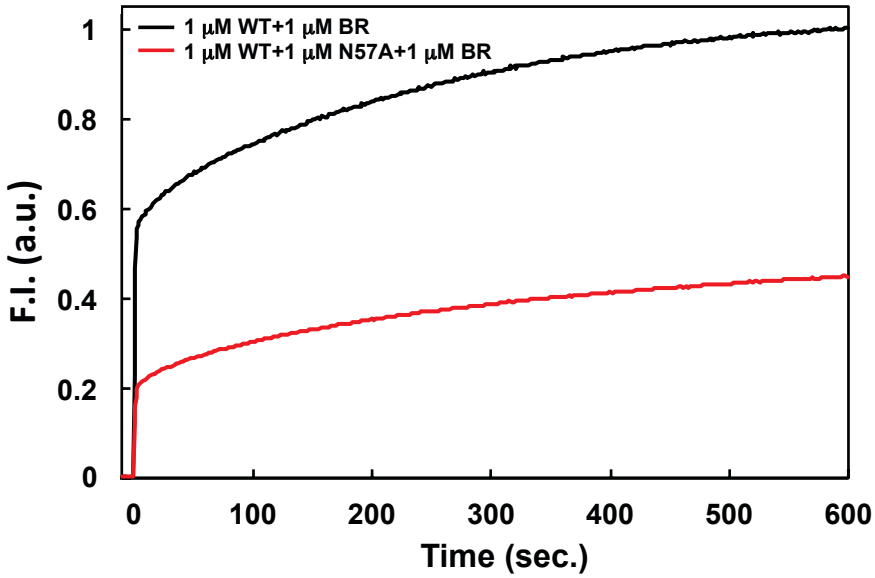

Figure 2.12. A comparison of FI time-courses between an equimolar mixture of WT holoUnaG and holo N57A mutant and the FI of 1 μM WT holoUnaG. The curves were normalized to the FI of WT UnaG at 10 min. Reprinted with permission from Yoh Shitashima, Togo Shimozawa, Akiko Kumagai, Atsushi Miyawaki, and Toru Asahi, Two distinct fluorescence states of the ligand-induced green fluorescent protein UnaG, *Biophysical Journal*, 113, 2805-2814 (2017) [4], Elsevier, copyright 2017. Consent from all authors has been secured.

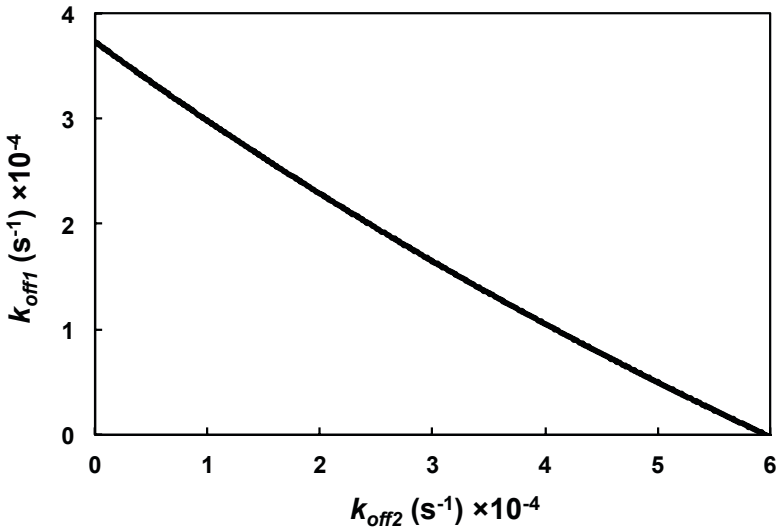

Figure 2.13. An example of relation between k_{off1} and k_{off2}. The possible values of (k_{off1}, k_{off2}) were expressed by points on the solid line, using the Equation (2.3) and the k_{off}, k_{12} and k_{21} values at the condition of 0 mM NaCl in Table 2.2. Reprinted with permission from Yoh Shitashima, Togo Shimozawa, Akiko Kumagai, Atsushi Miyawaki, and Toru Asahi, Two distinct fluorescence states of the ligand-induced green fluorescent protein UnaG, *Biophysical Journal*, 113, 2805-2814 (2017) [4], Elsevier, copyright 2017. Consent from all authors has been secured.

2.3.8 Effect of chloride ion concentration on interaction of UnaG and BR

The effects of solution conditions on the interaction properties of UnaG and BR were assayed by measuring the k, k_{on} and k_{off} at high chloride ion (K-Pi buffer containing 150 mM NaCl) in same manner as for the data in Figure 2.2, Figure 2.10 and Figure 2.11, and summarized in Table 2.2 to compare with the rates under the condition of 0 mM NaCl. I also examined FIDA for determining the distribution and brightness ratios of holoUnaG$_1$ and holoUnaG$_2$ at 150 mM NaCl. All rate constants were affected by chloride ion, although the distribution and the brightness ratios were not. The k_{on} was lowered by a factor of ~0.20 by increasing NaCl to 150 mM, whereas k and k_{off} were increased by factors of ~1.54 and 2.36, respectively.

Table 2.2. Kinetic rate constants of the UnaG and BR complex system with or without NaCl

Contents	NaCl 0 mM	NaCl 150 mM
k_{on}	7.05×10^{6} ($M^{-1}s^{-1}$)	1.42×10^{6} ($M^{-1}s^{-1}$)
k_{off}	2.17×10^{-4} (s^{-1})	5.13×10^{-4} (s^{-1})
k	4.34×10^{-3} (s^{-1})	6.69×10^{-3} (s^{-1})
k_{12}	1.72×10^{-3} (s^{-1})	2.66×10^{-3} (s^{-1})
k_{21}	2.62×10^{-3} (s^{-1})	4.03×10^{-3} (s^{-1})

The k_{12} and k_{21} were calculated from the apparent rate k using Equation (2.2), the brightness ratio (1:3.9) and the population ratio (60:40) of holoUnaG$_1$ and holoUnaG$_2$. Reprinted with permission from Yoh Shitashima, Togo Shimozawa, Akiko Kumagai, Atsushi Miyawaki, and Toru Asahi, Two distinct fluorescence states of the ligand-induced green fluorescent protein UnaG, *Biophysical Journal*, 113, 2805-2814 (2017) [4], Elsevier, copyright 2017. Consent from all authors has been secured.

2.4 Discussion

2.4.1 Dispersibility of UnaG and other fluorescent proteins

The dispersibility of FPs should be investigated to perform live cell fluorescence imaging correctly, because in most cases, the oligomer formation disturbs functions of labeled proteins, leading to abnormal cell behavior. For example, the DsRed derived from coral reefs tend to form strong tetramers, therefore the genetically-engineered monomeric versions of DsRed are preferred by current researchers for fluorescence imaging [10-12]. In this study, I demonstrated that both apoUnaG and holoUnaG are monomers even under conditions of high NaCl concentration, at least up to 7.5 μM. I also demonstrated that both apoUnaG and holoUnaG exist as monomeric forms in the presence of 1% w/v of PEG 6000, at least up to 6.5 μM (Figure 2.14). These facts indicated that both apoUnaG and holoUnaG exhibited monomeric dispersion in various conditions. However, it is known that the WT GFP forms a weak dimer at K_d = 0.11 mM [13], and the aggregation of the labeled proteins due to the dimerization of the WT GFP could disrupt cellular structures and functions [14]. From this perspective, the dispersibility of UnaG in higher concentrations should be examined further.

The differences between the experimental and theoretical MWs in this study (Figure 2.4) arose from an error in the *Vp*, one of the physical constants of proteins used in the fitting analysis. This is because the *Vp* of UnaG (0.721 cm^3/g) was estimated from the primary structure by SEDNTERP software, although the *Vp* values for proteins are affected by the conformation of the proteins. In fact, substituting the *Vp* for 0.708 cm^3/g can give the theoretical MW of UnaG, which is within the range of *Vp* values generally.

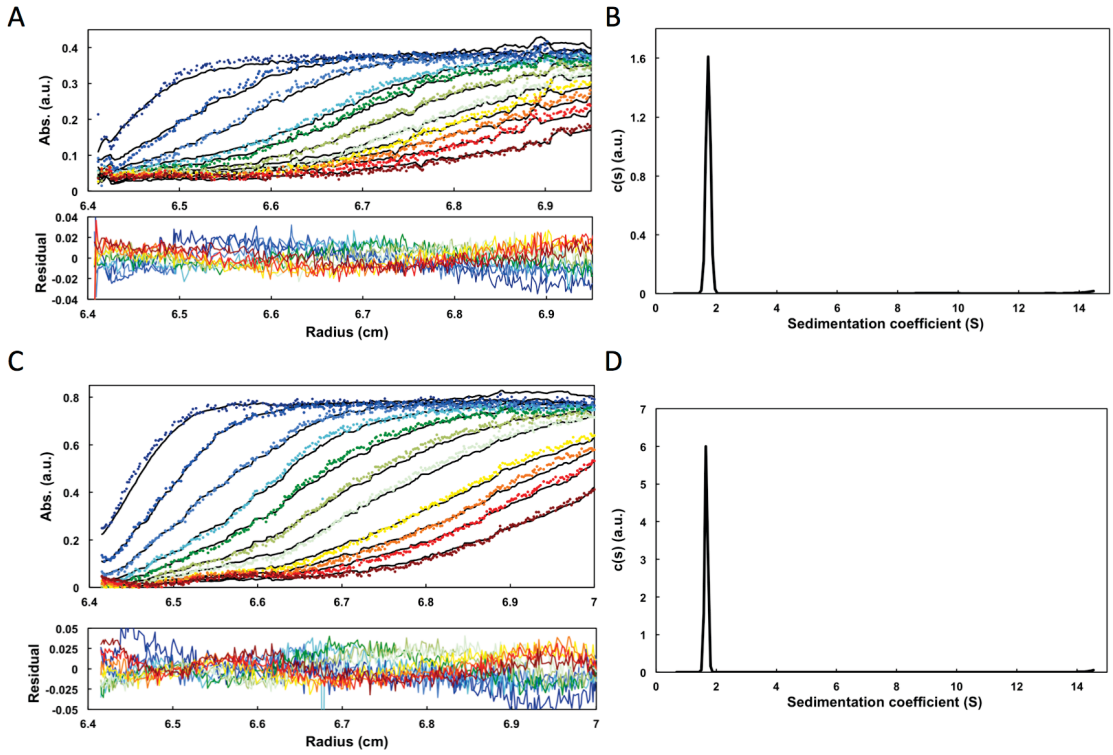

Figure 2.14. Sedimentation velocity analysis of apoUnaG and holoUnaG mixture in the presence of 1% w/v of PEG 6000. (A) Sedimentation velocity absorbance profiles, and (B) the c(s) as a result of the fitting analysis in graph (A) measured at 280 nm. (C) Sedimentation velocity absorbance profiles, and (D) the c(s) as a result of the fitting analysis in graph (C) measured at 500 nm. Both c(s) showed a single peak without a shoulder. Both apoUnaG and holoUnaG have the same sedimentation coefficients of ~1.7 S in the presence of 1% w/v of PEG 6000. Reprinted with permission from Yoh Shitashima, Togo Shimozawa, Akiko Kumagai, Atsushi Miyawaki, and Toru Asahi, Two distinct fluorescence states of the ligand-induced green fluorescent protein UnaG, *Biophysical Journal*, 113, 2805-2814 (2017) [4], Elsevier, copyright 2017. Consent from all authors has been secured.

2.4.2 The possibility of the transition between the two states in holoUnaG

At first, I assumed that the slow phase of the FI increase arose from additional BR binding to an unknown second ligand site in UnaG. This is because albumin such as BSA and HSA, which are well-known BR binding proteins, can both bind two BRs with different affinities [15, 16]. However, in the case of UnaG, the independence of the slow phase kinetics on the concentration of free BR indicated that the slow phase was not caused by additional BR binding. In addition, as spectroscopic studies in UnaG, the unchanged CD spectra during the slow phase also negated the possibility of a second BR binding site in UnaG, because the binding of free BR to UnaG and the resulting conformational fixation of BR inevitably caused the change in the CD spectrum [5, 17].

I next assumed a translocation or rearrangement of bound BR to another site with a change in brightness. I were aware that the liver-type FABP (FABP1), which has a high degree of homology and similar tertiary structure to UnaG, has a bound palmitic acid that causes translocation from the initial superficial site to a deeper site with a large conformational change [18]. However, in the case of UnaG, the unchanged CD spectra during the slow phase (Figure 2.8) indicated that the BR bound to holoUnaG did not alter its conformation, as seen in FABP1.

The kinetics of the slow phase (Figure 2.2) and the co-existence of the two states at the equilibrium state (Table 2.1) indicated that the slow phase was associated with a reversible intra-molecular reaction. It is well-known that some GFP family proteins have the protonation/deprotonation states of their fluorophores accompanying the change of absorption spectra [19-21]. In the case of holoUnaG, however, the unchanged shape of the absorption spectra during the slow phase (Figure 2.8) indicated that bound BR does not exchange protons, because the protonation/deprotonation of fluorophores

would be reflected in the shape of the absorption spectra between holoUnaG$_1$ and holoUnaG$_2$.

2.4.3 Proposed mechanisms of transition between the two states

The results of the spectroscopic analysis suggested that the reversible intra-molecular reaction was not associated with the chemical and conformational change of BR and UnaG (Figure 2.8). These results implied that the intra-molecular reaction was associated with a change in the environmental conditions surrounding BR. The effects of chloride ion on the k, k_{on} and k_{off} (Table 2.2) indicated that the electrostatic force may play important roles in the transition between holoUnaG$_1$ and holoUnaG$_2$ as well as the interaction of UnaG and BR. I also determine the effect of iodine ion on the k, k_{on} and k_{off}, and summarized in Table 2.3. Although the iodine ion affects the value of k compare to chloride ion (Figure 2.15), the effects of iodide ion were the same as chloride ion (Table 2.3). The effects on the k_{on} and k_{off} could be simply explained by the charge screening effect, where electrostatic attraction and binding affinity between UnaG and BR are reduced by the surrounding ions in a solution, as also observed in the interaction of adipocyte-type FABP and associated ligand [22]. On the other hand, the increase in k at higher chloride ion is highly suggestive of the involvement of electrostatics in the reversible intra-molecular reaction, because the increase in k indicate the reduction of energy barrier separating holoUnaG$_1$ and holoUnaG$_2$, for example, the activation energy of the intra-molecular reaction.

Based on the consideration described above, a bi-stable switch in the direction of a polar residue proximal to BR is one reasonable explanation of the reversible intra-molecular interaction and the resulting FI change. I speculated that a polar residue, not associated with BR but another atom in holoUnaG$_1$, could be associated with BR in holoUnaG$_2$ through hydrogen bonds or electrostatic interactions due to the bi-stable directional change, which is driven by thermal fluctuations over the energy barrier

separating the two states. In fact, the alternative direction of a polar residue proximal to fluorophore and the resulting alternative interaction network between fluorophore and proximal residues were observed in EGFP [23]. In general, these changes are reflected in the fluorescence QE of fluorophore. These include the changes in electronic state of fluorophore, stabilization/destabilization of fluorophore by altering the network of hydrogen bonds and other interactions [24], and hydration state of fluorophore [23, 25].

Arg57 is a potential candidate residue that may be associated with BR in this manner. As shown with the significant weak-fluorescence of N57A holoUnaG [5], the fluorescence QE of holoUnaG was sensitive to the relationship between Arg57 and BR. Moreover, N57A did not exhibit the slow phase of FI increase after binding BR (Figure 2.16). These results indicated that Arg57 plays a key role not only in the basal fluorescence efficiency of UnaG, but also in the transition between holoUnaG$_1$ and holoUnaG$_2$.

Table 2.3. Kinetic rate constants of the UnaG and BR complex system with or without halide (chloride or iodine ion)

Contents	Non-salt	NaCl 150 mM	KI 150 mM
k	4.34×10^{-3} (s^{-1})	6.69×10^{-3} (s^{-1})	14.6×10^{-3} (s^{-1})
k_{on}	7.05×10^{6} ($M^{-1}s^{-1}$)	1.42×10^{6} ($M^{-1}s^{-1}$)	2.13×10^{6} ($M^{-1}s^{-1}$)
k_{off}	2.17×10^{-4} (s^{-1})	5.13×10^{-4} (s^{-1})	2.76×10^{-4} (s^{-1})

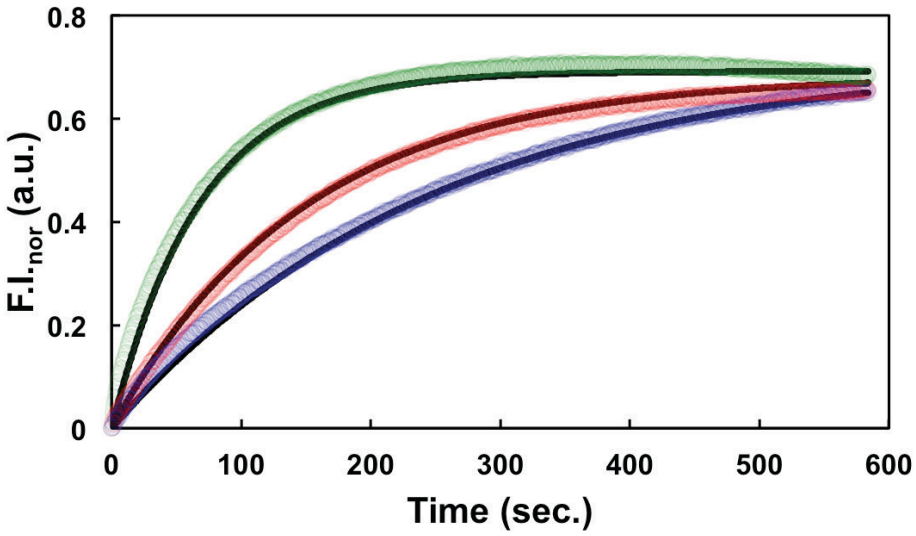

Figure 2.15. Normalized FI time-courses in the slow phase (colored dots) with fitting curves achieved by using Equation (2.1) (black line).

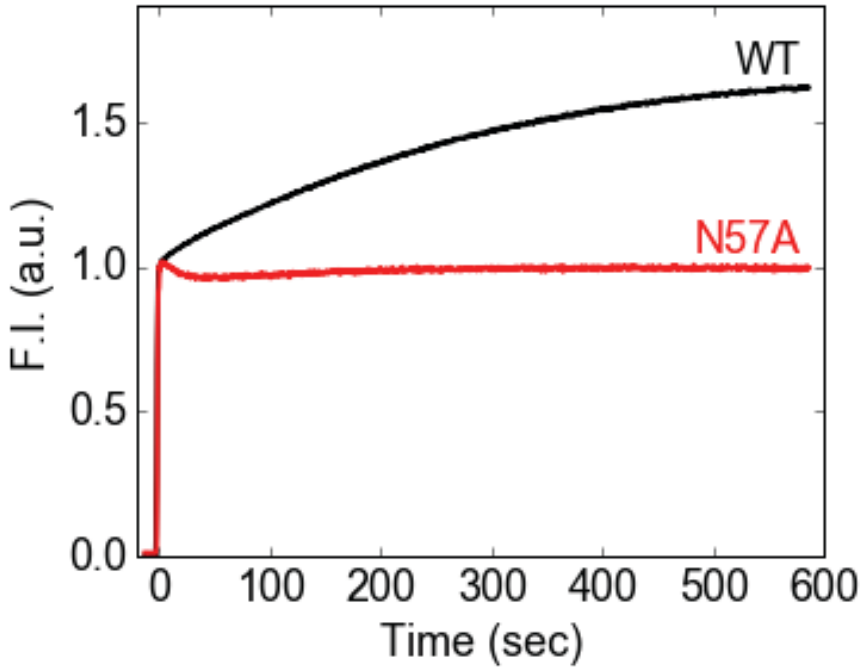

Figure 2.16. Normalized FI time-courses after mixing WT/N57A UnaG and BR. Excess amounts of BR (5 μM in final conc.) were added to 1 μM of WT or N57A apoUnaG solution at t = 0. The curves were normalized to the amplitude of rapid phase on the FI increase (FI_0). Reprinted with permission from Yoh Shitashima, Togo Shimozawa, Akiko Kumagai, Atsushi Miyawaki, and Toru Asahi, Two distinct fluorescence states of the ligand-induced green fluorescent protein UnaG, *Biophysical Journal*, 113, 2805-2814 (2017) [4], Elsevier, copyright 2017. Consent from all authors has been secured.

2.5 Conclusion

In conclusion, I have demonstrated that holoUnaG exhibits two different fluorescence intensities. From FIDA result, I determined that holoUnaG$_1$ was gradually converted to holoUnaG$_2$, which acquired 3.9 times higher brightness, and finally both holoUnaG$_1$ and holoUnaG$_2$ reached equilibrium state with an average holoUnaG$_1$/holoUnaG$_2$ ratio of 60:40. I reasoned that slight conformational changes of amino acid residues around ligand-binding site would induce the changes from holoUnaG$_1$ to holoUnaG$_2$; especially the N57 is a key residue that triggers these changes. I also determined the association and dissociation rate constants between UnaG and BR, and provided a novel schema of the UnaG and BR complex system.

The findings of this study provide key information for the practical use of UnaG. For example, when I quantify the amount of BR *in vitro* or *in vivo* from the fluorescence signal of holoUnaG, the equilibration time (several minutes) for the two states must be taken into account. The quantum efficiency (QE) of holoUnaG has been reported as 51% [5], although this was measured at equilibrium for the two states. The individual QEs of holoUnaG$_1$ and holoUnaG$_2$ correspond to 23% and 92% respectively, according to their distribution at equilibrium (60:40) and the molecular brightness ratio (1:3.9) determined in this study. I suggest that the QE of holoUnaG$_2$ is the highest value for BR. The discovery of a higher QE for holoUnaG$_2$ opens the possibility for the development of a brighter UnaG with the construction of a constitutive holoUnaG$_2$ by genetic engineering.

2.6 References

1. Ando, R., H. Hama, M. Yamamoto-Hino, H. Mizuno, and A. Miyawaki, "An optical marker based on the UV-induced green-to-red photoconversion of a fluorescent protein", *Proc. Natl. Acad. Sci. U.S.A.,* **99**, 12651-12656 (2002).
2. Ando, R., H. Mizuno, A. Miyawaki, "Regulated Fast Nucleocytoplasmic Shuttling Observed by Reversible Protein Highlighting", *Science*, **306**, 1370-1373 (2004).
3. Iizuka, R., M. Yamagishi-Shirasaki, and T. Funatsu, "Kinetic study of de novo chromophore maturation of fluorescent proteins", *Anal. Biochem.*, **414**, 173-178 (2011).
4. Shitashima, Y., T. Shimozawa, A. Kumagai, A. Miyawaki, and T. Asahi, "Two distinct fluorescence states of the ligand-induced green fluorescent protein UnaG", *Biophys. J.*, **113**, 2805-2814 (2017).
5. Kumagai, A., R. Ando, H. Miyatake, P. Greimel, T. Kobayashi, Y. Hirabayashi, T. Shimogori, and A. Miyawaki, "A bilirubin-inducible fluorescent protein from eel muscle", *Cell*, **153**, 1602–1611 (2013).
6. Lebowitz, J., M. S. Lewis, and P. Schuck, "Modern analytical ultracentrifugation in protein science: a tutorial review", *Protein Sci.*, **11**, 2067–2079 (2002).
7. Schuck, P., M. A. Perugini, N. R. Gonzales, G. J. Howlett, and D. Schubert, "Size-Distribution Analysis of Proteins by Analytical Ultracentrifugation: Strategies and Application to Model Systems", *Biophys. J.*, **82**, 1096–1111 (2002).
8. Kask, P., K. Palo, D. Ullmann, and K. Gall, "Fluorescence-intensity distribution analysis and its application in biomolecular detection technology", *Proc. Natl.*

Acad. Sci. U. S. A., **96**, 13756–13761 (1999).

9. Kask, P., K. Palo, N. Fay, L. Brand, Ü. Mets, D. Ullmann, J. Jungmann, J. Pschorr, and K. Gall, "Two-Dimensional Fluorescence Intensity Distribution Analysis: Theory and Applications", *Biophys. J.*, **78**, 1703–1713 (2000).
10. Baird, G. S., D. A. Zacharias, and R. Y. Tsien, "Biochemistry, mutagenesis, and oligomerization of DsRed, a red fluorescent protein from coral", *Proc. Natl. Acad. Sci. U. S. A.*, **97**, 11984–11989 (2000).
11. Campbell, R. E., O. Tour, A. E. Palmer, P. A. Steinbach, G. S. Baird, D. A. Zacharias, and R. Y. Tsien, "A monomeric red fluorescent protein", *Proc. Natl. Acad. Sci. U. S. A.*, **99**, 7877–7882 (2002).
12. Shaner, N. C., R. E. Campbell, P. A. Steinbach, B. N. Giepmans, A. E. Palmer, and R. Y. Tsien, "Improved monomeric red, orange and yellow fluorescent proteins derived from Discosoma sp. red fluorescent protein", *Nat. Biotechnol.*, **22**, 1567–1572 (2004).
13. Zacharias, D. A., J. D. Violin, A. C. Newton, and R. Y. Tsien, "Partitioning of lipid-modified monomeric GFPs into membrane microdomains of live cells", *Science*, **296**, 913–916 (2002).
14. Segami, S., S. Makino, A. Miyake, M. Asaoka, and M. Maeshima, "Dynamics of Vacuoles and H^+-Pyrophosphatase Visualized by Monomeric Green Fluorescent Protein in Arabidopsis: Artifactual Bulbs and Native Intravacuolar Spherical Structures, *Plant Cell Online*, **26**, 3416–3434 (2004).
15. Goncharova, I., S. Orlov, and M. Urbanová, "The location of the high- and low-affinity bilirubin-binding sites on serum albumin: Ligand-competition analysis investigated by circular dichroism", *Biophys. Chem.*, **180–181**, 55–65

(2013).

16. Goncharova, I., S. Orlov, and M. Urbanová, “Chiroptical properties of bilirubin-serum albumin binding sites”, *Chirality*, **25**, 257–263 (2013).

17. Pimenta, F. M., J. K. Jensen, M. Etzerodt, and P. R. Ogilby, “Protein-encapsulated bilirubin: paving the way to a useful probe for singlet oxygen”, *Photochem. Photobiol. Sci.*, **14**, 665–677 (2015).

18. Sharma, A., and A. Sharma, “Fatty acid induced remodeling within the human liver fatty acid-binding protein”, *J. Biol. Chem.*, **286**, 31924–31928 (2011).

19. Heim, R., D. C. Prasher, and R. Y. Tsien, “Wavelength mutations and posttranslational autoxidation of green fluorescent protein”, *Proc. Natl. Acad. Sci. U. S. A.*, **91**, 12501–12504 (1994).

20. Habuchi, S., R. Ando, P. Dedecker, W. Verheijen, H. Mizuno, A. Miyawaki, and J. Hofkens, “Reversible single-molecule photoswitching in the GFP-like fluorescent protein Dronpa”, *Proc. Natl. Acad. Sci. U. S. A.*, **102**, 9511–9516 (2005).

21. Higashino, A., M. Mizuno, and Y. Mizutani, “Chromophore Structure of Photochromic Fluorescent Protein Dronpa: Acid-Base Equilibrium of Two Cis Configurations”, *J. Phys. Chem. B.*, **120**, 3353–3359 (2016).

22. Schoeffler, A. J., C. R. Ruiz, A. M. Joubert, X. Yang, and V. J. LiCata, “Salt modulates the stability and lipid binding affinity of the adipocyte lipid-binding proteins”, *J. Biol. Chem.*, **278**, 33268–33275 (2003).

23. Arpino, J. A. J., P. J. Rizkallah, and D. D. Jones, “Crystal Structure of Enhanced Green Fluorescent Protein to 1.35 Å Resolution Reveals Alternative Conformations for Glu222”, *PLoS One*, **7**, e47132 (2012).

24. Goedhart, J., D. von Stetten, M. Noirclerc-Savoye, M. Lelimousin, L. Joosen, M. A. Hink, L. van Weeren, T. W. Gadella, and A. Royant, “Structure-guided evolution of cyan fluorescent proteins towards a quantum yield of 93%”, *Nat. Commun.*, **3**, 751 (2012).

25. Lehtivuori, H., S. Bhattacharya, N. M. Angenent-Mari, K. A. Satyshur, and K. T. Forest, “Removal of Chromophore-Proximal Polar Atoms Decreases Water Content and Increases Fluorescence in a Near Infrared Phytofluor”, *Front. Mol. Biosci.*, **2**, 65 (2015).

Chapter 3

A Ca^{2+}-dependent Bilirubin Releasing Protein Based on UnaG

3.1 Introduction

In Chapter 2, I described important molecular properties of UnaG for their use as FPs, such as the association/dissociation rate constants of ligands and their dispersion in aqueous solution. This study provides us the information of the practical use of UnaG; for example, (i) UnaG do not express self-aggregation under several conditions, at least up to 7.5 μM, and (ii) relatively low k_{off} value of ligands would provide the high affinity of ligand to UnaG. For next challenge, I attempted to generate novel functional protein based on UnaG. I focused on the ligand of UnaG, bilirubin (BR), which has attracted in the physiological field for decades. Since it is well known that excess accumulation of BR causes several clinical symptoms such as jaundice, BR has been an important diagnostic index in clinical medicine [1, 2]. On the other hand, BR containing a reactive hydrogen atom and conjugated double bonds is known to be a notable antioxidant scavenger for reactive oxygen species (ROS) in biological tissues [3, 4], especially in biological membranes. Therefore, optimal regulation of BR concentrations in biological tissues could steer clinical therapies for aging, as well as avoiding the risk of certain diseases that are caused by BR accumulation. However, UnaG hardly releases BR because of the very high affinity interaction involving UnaG and BR, especially its low k_{off} value.

The purpose in chapter 3 is to engineer the binding of UnaG to be sensitive to free calcium ion. I attempted to engineer the BR binding of UnaG to be sensitive to free Ca^{2+}. The strategy of designing the protein was devised from the single fluorescent protein-based indicator (SFPBI) [5]. I speculated that the insertion of calmodulin (CaM)

near the BR binding pocket of UnaG would result in the production of a novel fluorescent protein that releases the fluorophore in a Ca^{2+}-dependent manner. This is because that one of the SFPBI, Camgaroo1 [6], was generated by insertion of CaM into Enhanced yellow fluorescent protein (EYFP) and the generated protein could change its fluorescent intensity (FI) by Ca^{2+}. Recently, To et al. developed the "UnaG-based protein-protein interaction reporter (uPPI)" by using the protein-fragment complementation approach[7]. They revealed that the site between residues 84 and 85 of UnaG was tolerant to protein insertion. In addition, as the site was close to Ser80/Asp81 residues, Ca^{2+}-dependent conformational change due to CaM insertion was expected to affect the anchoring of the propionate carboxylate from exo-vinyl dipyrrinone.

Remarkably, one of the UnaG/CaM chimeric proteins constructed in this study, termed BReleaCa (indicating BR + releaser + Ca^{2+}), decreased BR affinity and accordingly the green fluorescence intensity (FI) markedly with Ca^{2+}. I investigated the association/dissociation kinetics between BReleaCa and BR by monitoring fluorescence as the readout and provide mechanical insights into the interplay between BR and Ca^{2+} on the dual-ligand-modulable protein.

This part is reproduced with permission from Yoh Shitashima, Togo Shimozawa, Toru Asahi, and Atsushi Miyawaki, A dual-ligand-modulable fluorescent protein based on UnaG and calmodulin, *Biochemical and Biophysical Research Communications*, 496, 872-879 (2018) [8], Elsevier, copyright 2018. Consent from all authors has been secured.

3.2 Experimental Section

3.2.1 Chemicals

Bilirubin (BR), dimethylsulfoxide (DMSO), and ampicillin sodium were purchased from Wako Pure Chemicals Industries, Ltd. (Osaka, Japan). Isopropyl-β-D-thiogalactopyranoside (IPTG) was purchased from Carbosynth Ltd. (Berkshire, U.K.). HEPES was purchased from Dojindo Lab. (Kumamoto, Japan). Ethylene glycol-bis(β-aminoethyl ether)-N,N,N',N'-tetraacetic acid tetrasodium salt (EGTA-Na) was purchased from Sigma-Aldrich Co. LLC (St. Louis, MO, U.S.A.). Calcium Calibration Buffer Kit #1 was purchased from Thermo Fisher Scientific (Waltham, MA, U.S.A.). BR was dissolved in DMSO at 1 mM or at 25 mM, and stored at −20°C until use.

3.2.2 Preparation of Proteins

Calmodulin (*CaM*) and *mCherry* were acquired from Addgene plasmid 40753, and 35687, respectively (Cambridge, MA, U.S.A.). pColdI-UnaG was prepared as described in Chapter 2 [9]. To create *BReleaCa*, *CaM* was inserted into *UnaG* between residues 84 and 85 with both ends employing tetrapeptide linkers (GGSG-CaM-GGSG) at the 19-bp overlapping sequences by a SLiCE reaction [10, 11], resulting in pColdI-BReleaCa. BReleaCa expression and purification were performed as described in Chapter 2[9] with changing K-Pi buffer (20 mM potassium phosphate buffer adjusted to pH 7.5) to HEPES buffer (100 mM HEPES buffer containing 150 mM NaCl, adjusted to pH 7.5). Although I used the purified 6x His-BReleaCa without digestion of the 6x His-tag, I refer to 6x His-UnaG as BReleaCa for simplification of the description in this study.

3.2.3 Spectroscopic Studies

The measurements of excitation and fluorescence spectra and FI time-course of BReleaCa were performed using an RF-5300PC spectrophotometer (Shimadzu, Kyoto, Japan), and an F-2500 spectrophotometer (Hitachi Ltd., Tokyo, Japan). For the measurements of the FI time-course, BR titration experiments, and measuring K_d, the excitation and emission wavelength were set at 490 nm and 525 nm, respectively. Absorption spectra were recorded using a V-660 spectrophotometer (JASCO Corporation, Tokyo, Japan). The formation of BReleaCa binding to BR (BR-BReleaCa) was triggered by the addition of a small volume of high concentration BR dissolved in DMSO (1 mM or 25 mM) to 2 ml BReleaCa in a 10 mm path quartz cuvette. For changing internal Ca^{2+} concentration, calcium chloride ($CaCl_2$) or EGTA-Na (pH 7.5) dissolved in ultra pure water (1 M each) were added. The measurements of dissociation rate constants were performed using an RF-5300PC spectrophotometer (Shimadzu, Kyoto, Japan). As described previously, the FI of BR-BReleaCa was monitored after the addition of a nonfluorescent BR scavenger UnaG(N57A) [8].All data other than those for K_d were collected at room temperature. K_d data were collected at 20°C.

3.2.4 Stopped-flow Analysis

The measurements of association rate constants were performed using an SX20 Stopped-Flow Spectrometer (Applied Photophysics, Leatherhead, U.K.). Equal volumes of a 2 μM BReleaCa solution and a 2 μM BR solution were rapidly mixed, and thus the total concentrations of BReleaCa and BR ($[BReleaCa]_t$ and $[BR]_t$, respectively) were both 1 μM. Since the fluorescence of BR-BReleaCa is considerably bright, it is possible to reproducibly characterize the rapid increase in FI (dFI/dt), which should be

proportional to the initial rate of the generation of BR-BReleaCa (d[BR-BReleaCa]/dt). In principle, I calculated k_{on} using the relationship: d[BR-BReleaCa]/dt = k_{on} ×[BReleaCa]$_t$ × [BR]$_t$. To convert measured FI into [BR-BReleaCa], I performed some stoichiometry calculations. First, I determined the steady state values of [BR-BreleaCa] using $K_{d\ (Ca^{2+}(-))}$ and $K_{d\ (Ca^{2+}(+))}$. Then, assuming that the entire process of fluorescence development is composed of a rapid and a slow phases as was shown with UnaG [8], I calculated the maximum [BR-BReleaCa] values given by the rapid phase. All data were collected at a room temperature.

3.2.5 Cell Culture and Transfection

To generate *BReleaCa-mCherry* for expression in HeLa S3 cells, *BReleaCa* and *mCherry* were assembled by a SLiCE reaction at the C terminus of *BReleaCa* with a nonapeptide linker (GGSGGSGGS). *BReleaCa-mCherry* was cloned into the pcDNA3 vector between the *EcoR*I and *Xba*I restriction sites using a SLiCE reaction. Cells were passaged in low-glucose Dulbecco's modified Eagle's medium (DMEM) supplemented with 10% fetal bovine serum (FBS) and 0.1% penicillin-streptomycin. HeLa S3 cells, grown in 35 mm glass-based dishes, were transiently transfected with pRK5-HA-BReleaCa-mCherry plasmid (1 mg per dish) using polyethylenimine (PEI, 2 μl per 1 mg DNA). Transfection was performed when cells were cultured to ~60-70% confluence, and cells were imaged around 24 h after transfection.

3.2.6 Fluorescent Microscopy

Transfected HeLa S3 cells were imaged in 35 mm glass-based dishes using an IX70 inverted microscope (Olympus Corporation, Tokyo, Japan) with a standard 75-W

xenon lamp, a 20x air objective lens (UPlanSApo, numerical aperture 0.70), and a CoolSNAP HQ2 CCD camera (Photometrics, Tucson, AZ, U.S.A.). Optical filters were automated using Lambda 10-2 hardware (Sutter instruments Co., Novato, CA, U.S.A.) with the following excitation and emission filters: 485DF15-nm/530DF30-nm for BReleaCa imaging, and 550DF30-nm/590DF35-nm for mCherry imaging, excitation/emission respectively. A 455DRLP dichroic mirror and 33% neutral density filter (N.D.3) was typically used. Before imaging, samples were prepared as follows: (i) removal of DMEM, (ii) washing of the cells with phosphate buffered saline (PBS) containing 1 mM ethylendiaminetetraacetic acid (EDTA), (iii) adding Hanks' balanced salt solution without calcium and magnesium (HBSS(-)) containing 100 μM EGTA-Na and 100 nM BR, (iv) washing extracellular BR out, (v) standing over 15 min at atmosphere. For changing intracellular Ca^{2+} concentration, 1 mM $CaCl_2$ containing 1 μM ionomycin, or 2 mM EGTA-Na were added. Images were acquired with exposure times of 200 ms for BReleaCa and 500 ms for mCherry, respectively. Data were collected at room temperature. The whole system was controlled using MetaFluor software (Molecular Devices, Sunnyvale, CA, U.S.A.). Images were analyzed using the ImageJ software (NIH, Bethesda, MD, U.S.A.).

3.3 Results

3.3.1 Fusion of CaM to UnaG

In this study, I attempted to insert CaM into UnaG at the site between residues 84 and 85 (Figure 3.1). I first designed two chimeric proteins (Figure 3.2, #1, 2) by inserting CaM-derived peptides with tetrapeptide linkers (GGSG) into UnaG [12] at the site between residues 84 and 85. A previous study showed that the site was tolerant of insertion of foreign proteins [7]. However, insertion of a 29 amino acid peptide or a 12 amino acid peptide containing the 3rd calcium binding region of CaM (III) resulted in a significant misfolding of UnaG. Then I substituted a whole CaM protein for the insert (Figure 3.2, #3) and was able to make UnaG fold well. After expression in *E coli*, protein #3 was affinity-tag purified for reconstitution with BR. The addition of 1 μM BR in the presence of 100 μM EGTA-Na elicited an immediate development of green fluorescence that reached a plateau in approximately 20 min (Figure 3.3A, BR 1 μM). Interestingly, however, a subsequent addition of 200 μM $CaCl_2$ quenched the fluorescence rapidly to nearly zero (Figure 3.3A, $CaCl_2$ 200 μM). It was speculated that the conversion from apo-CaM to holo-CaM induced either the dissociation of BR from UnaG or the decrease of the fluorescence quantum yield of UnaG.

To discriminate these two possibilities, I next performed absorption measurements. It is known that free and UnaG-bound BR molecules absorb light maximally at 448 nm (ε = 55,000 $M^{-1}cm^{-1}$) and 498 nm (ε = 77,300 $M^{-1}cm^{-1}$) [13]. The absorption spectra in the presence and absence of free Ca^{2+} were characterized exclusively by 448- and 494- nm peaks, respectively (Figure 3.3B, C), suggesting that the Ca^{2+}-saturated chimeric protein had no bound BR in the ligand cavity. As protein #3 appeared to release BR in response to Ca^{2+}, I named it “BReleaCa”. Importantly, I was

able to restore the BR binding (Figure 3.3A, EGTA 400 μM) for a subsequent BR release again (Figure 3.3A, $CaCl_2$ 400 μM) by controlling free Ca^{2+} concentrations, confirming the reversible performance of BReleaCa.

I also tried using a CaM-M13 hybrid protein as the insert (Figure 3.2, #4). Furthermore, as residues 84 and 85 of UnaG are a site that tolerates circular permutation where two portions of the polypeptide are flipped around [14], I generated constructs in which circularly permuted UnaG (cp85UnaG) was sandwiched by CaM and M13 (Figure 3.2, #5, 6). However, neither of them folded well enough for BR incorporation.

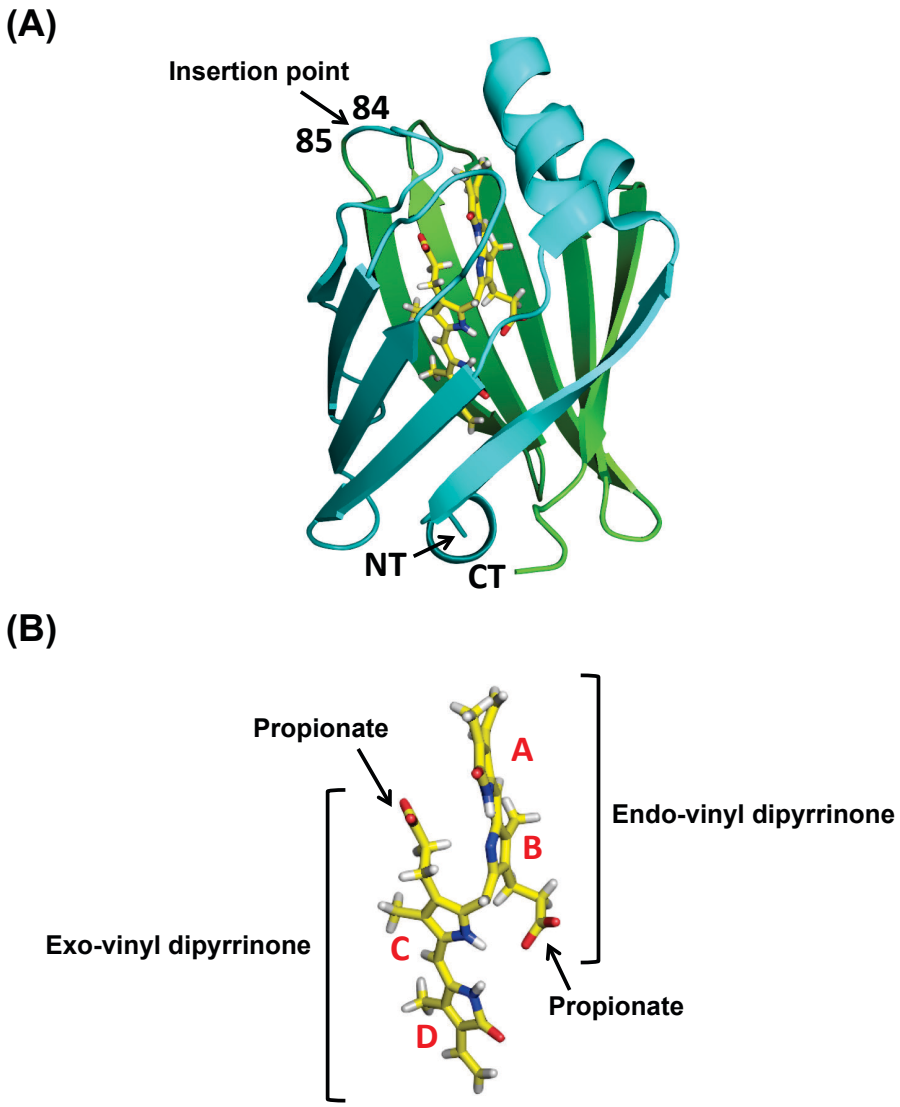

Figure 3.1. Crystallographic structure of holoUnaG. (A) Overall structure of UnaG-BR complex. The site between residues 84 and 85 for insertion of foreign peptides is indicated. The image was created using PyMol (DeLano Scientific) from PDB file 4I3B[13]. **(B)** The bound BR in (A). BR is shown as a stick representation with atoms colored (carbon, yellow; oxygen, red; nitrogen, blue; hydrogen, gray). Rings A/B and rings C/D compose the *endo*-vinyl dipyrrinone and *exo*-vinyl dipyrrinone moieties. NT, amino terminus. CT, carboxyl terminus. Reprinted with a modification and with permission from Yoh Shitashima, Togo Shimozawa, Toru Asahi, and Atsushi Miyawaki, A dual-ligand-modulable fluorescent protein based on UnaG and calmodulin, *Biochemical and Biophysical Research Communications*, 496, 872-879 (2018) [8], Elsevier, copyright 2018. Consent from all authors has been secured.

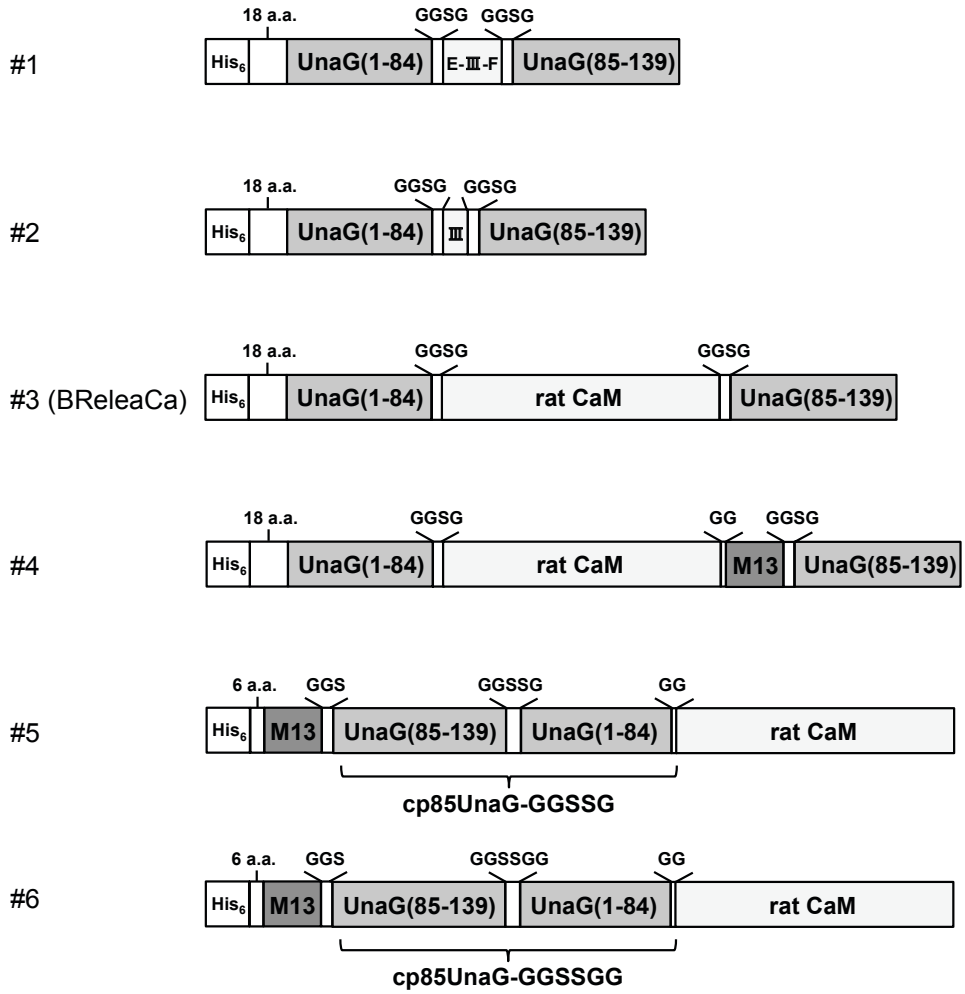

Figure 3.2. Schematic domain structures and sequences of UnaG/CaM hybrid proteins for expression in *E. coli.* Amino acid compositions (G, glycine; S, serine) of linkers are shown above the structures. His_6, hexa-histidine tag. (#1) E-III-F: a 29 amino acid peptide containing the 3rd calcium binding region of rat CaM. (#2) III: a 12 amino acid peptide containing the 3rd calcium binding region of rat CaM. (#3) Insertion of the entire protein of rat CaM. This protein was further characterized as BReleaCa in the present study. (#4) Insertion of CaM-M13. (#5) cp85UnaG-GGSSG was generated by linking the original N and C termini through a penta-peptide linker (GGSSG), rendering residues 85 and 84 new N and C termini, respectively. (#6) cp85UnaG-GGSSGG was generated by linking the original N and C termini through a hexa-peptide linker (GGSSGG), rendering residues 85 and 84 new N and C termini, respectively. Reprinted with a modification and with permission from Yoh Shitashima, Togo Shimozawa, Toru Asahi, and Atsushi Miyawaki, A dual-ligand-modulable fluorescent protein based on UnaG and calmodulin, *Biochemical and Biophysical Research Communications*, 496, 872-879 (2018) [8], Elsevier, copyright 2018. Consent from all authors has been secured.

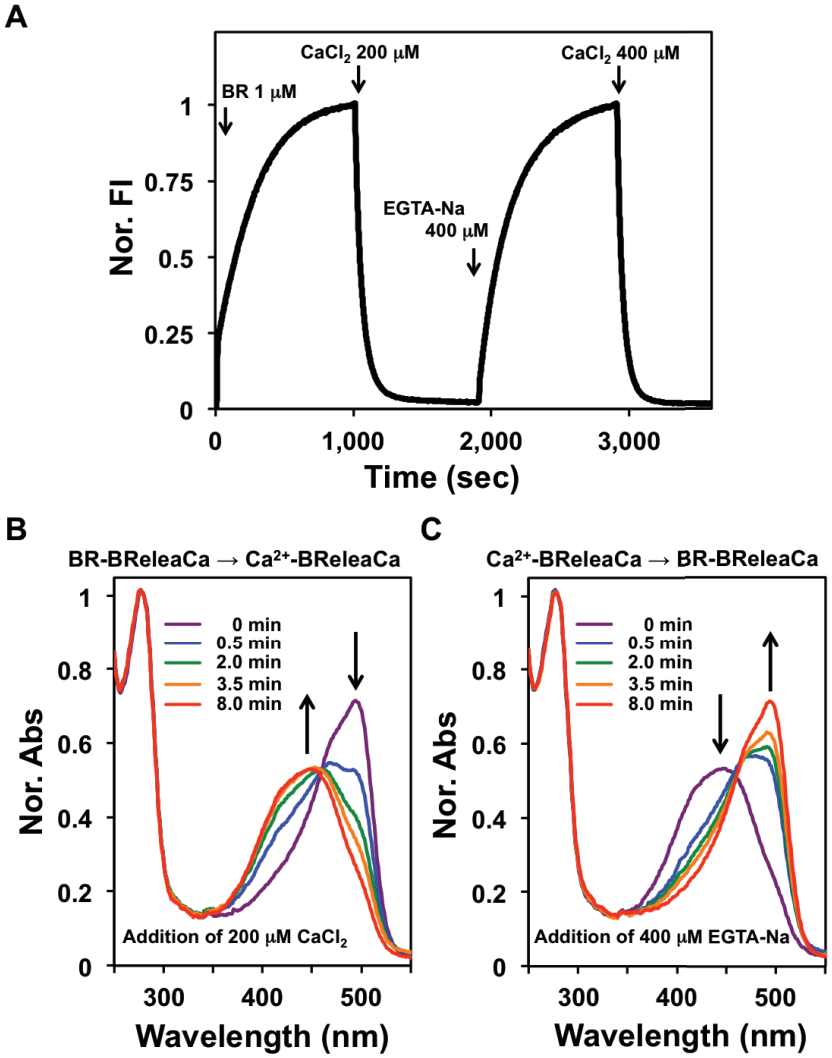

Figure 3.3. BReleaCa: A fluorescent protein that releases BR reversibly in a Ca^{2+}-dependent manner. (**A**) A time course of intensity of fluorescence from a 2 ml solution containing 1 μM BReleaCa and initially 100 μM EGTA-Na. Then, a 4 μl solution of 100 mM $CaCl_2$, an 8 μl solution of 100 mM EGTA-Na, and an 8 μl solution of 100 mM $CaCl_2$ were sequentially added. Final concentrations of the added solutes are indicated. **(B)** Absorption spectra of BReleaCa during the transition process from the Ca^{2+}-depleted to Ca^{2+}-saturated forms. **(C)** Absorption spectra of BReleaCa during the transition process from the Ca^{2+}-saturated to Ca^{2+}-depleted forms. (B, C) As was done in the experiment of (A), $CaCl_2$ and EGTA-Na (final conc. 200 μM and 400 μM, respectively) were sequentially added after reconstitution of BReleaCa with BR. Reprinted with permission from Yoh Shitashima, Togo Shimozawa, Toru Asahi, and Atsushi Miyawaki, A dual-ligand-modulable fluorescent protein based on UnaG and calmodulin, *Biochemical and Biophysical Research Communications*, 496, 872-879 (2018) [8], Elsevier, copyright 2018. Consent from all authors has been secured.

3.3.2 BReleaCa: a fluorescent protein that releases BR upon Ca^{2+} binding

A hypothetical kinetic model for the association/dissociation of BR and Ca^{2+} with BReleaCa is shown in Figure 3.4. I first monitored the absorption spectrum during the transition from BR-BReleaCa to Ca^{2+}-BReleaCa (Figure 3.3B). The time course was very similar to that observed for fluorescence (Figure 3.3A, $CaCl_2$ 200 μM). Moreover, a clear isosbestic point at 460 nm was noted (Figure 3.3B), which suggests equilibrium between the 448- and 494- nm absorbing species (BR-BReleaCa and Ca-BReleaCa, respectively). Taken together, it was assumed that the fraction of Ca^{2+}-BR-BReleaCa (Figure 3.4, bottom), which may have a distinct spectroscopic property, is negligible.

I also monitored the absorption spectrum during the transition from Ca^{2+}-BReleaCa to BR-BReleaCa (Figure 3.3C). However, no clear isosbestic point was observed, suggesting a rather complex mechanism for the reconstitution of BReleaCa (Figure 3.4, top) with BR. In fact, I have shown that the reconstitution of apoUnaG with BR consists of a rapid generation of a moderately fluorescent species and a slow maturation process towards the bright holoUnaG [9].

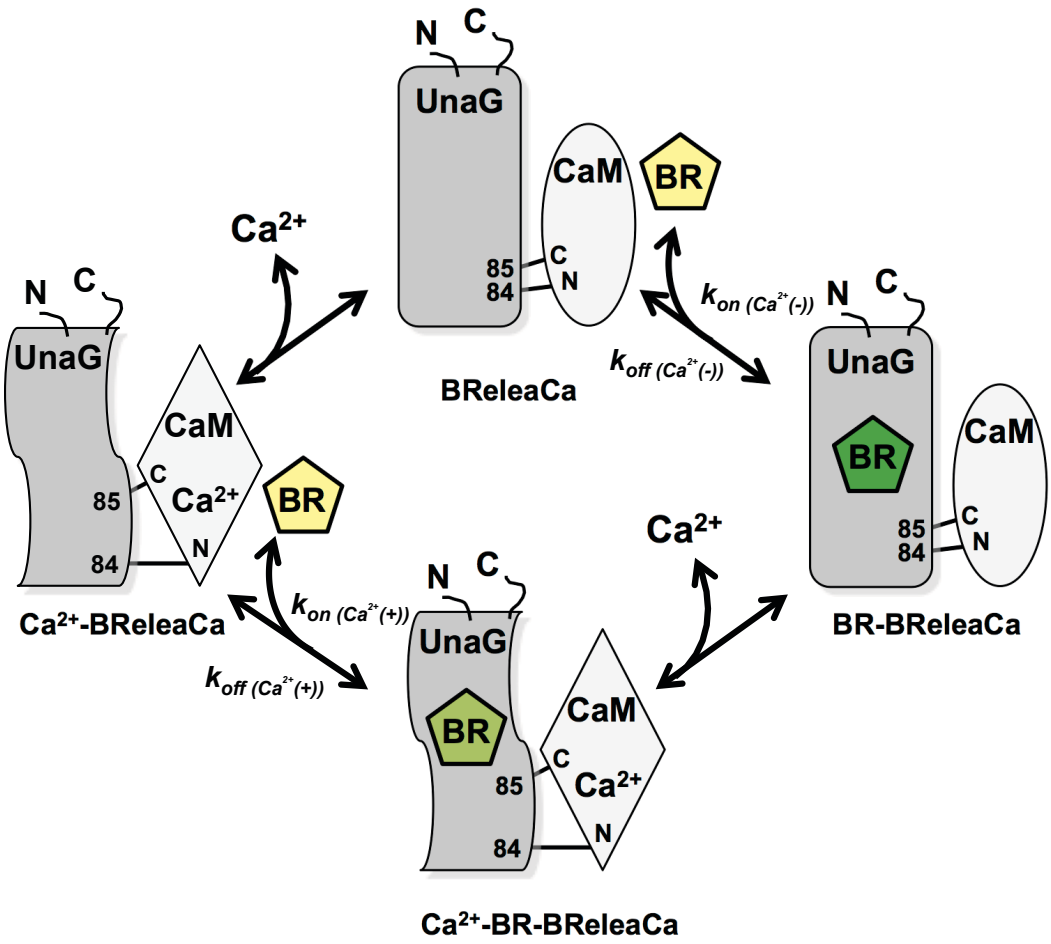

Figure 3.4. Schematic model of the BR- and Ca^{2+}-binding of BReleaCa. BReleaCa (top) is the apo-protein generated by bacteria and depleted of Ca^{2+} ion. It is ready for reconstitution with BR to become BR-BReleaCa (right), which emits bright green fluorescence. BR-BReleaCa is converted by Ca^{2+} ion to non-fluorescent Ca^{2+}-BReleaCa (left) via Ca^{2+}-BR-BReleaCa (bottom), which may show a very short lifetime and yet uncharacterized fluorescence. N, amino terminus. C, carboxyl terminus. Reprinted with permission from Yoh Shitashima, Togo Shimozawa, Toru Asahi, and Atsushi Miyawaki, A dual-ligand-modulable fluorescent protein based on UnaG and calmodulin, *Biochemical and Biophysical Research Communications*, 496, 872-879 (2018) [8], Elsevier, copyright 2018. Consent from all authors has been secured.

3.3.3 The dissociation constant of BReleaaca and BR

FI measurement makes it possible to examine the equilibrium state of BReleaCa. I determined the dissociation constants for BR binding in the presence ($K_{d\,(Ca^{2+}(+))}$) and absence ($K_{d\,(Ca^{2+}(-))}$) of Ca^{2+} by monitoring FI in BR titration experiments. Equation 3.1 was used to fit the date points (see the derivation of the equation 3.1):

$$\frac{P_c}{P_t} = \frac{\left(K_d + B_t + P_t\right) - \sqrt{\left(K_d + B_t + P_t\right)^2 - 4 \cdot B_t \cdot P_t}}{2 \cdot P_t} \quad \cdots \text{Equation (3.1)}$$

where K_d is the dissociation constant, B_t is the total BR concentration, P_t is the total protein concentration, and P_c is the concentration of ligand bound protein. $K_{d\,(Ca^{2+}(-))}$ and $K_{d\,(Ca^{2+}(+))}$ were determined to be 9.70 nM (Figure 3.5, blue) and 9.65 μM (Figure 3.5, red), respectively. The latter curve suggests the existence of a fluorescent species at high Ca^{2+}-concentrations: Ca^{2+}-BR-BReleaCa (Figure 3.4). It was therefore concluded that the affinity of BReleaCa for BR ($K_{d\,(Ca^{2+}(-))}$ = 9.70 nM) was approximately 100-fold weaker than that of UnaG (98 pM) but approximately 1,000-fold stronger than that of Ca^{2+}-BReleaCa ($K_{d\,(Ca^{2+}(+))}$ = 9.65 μM).

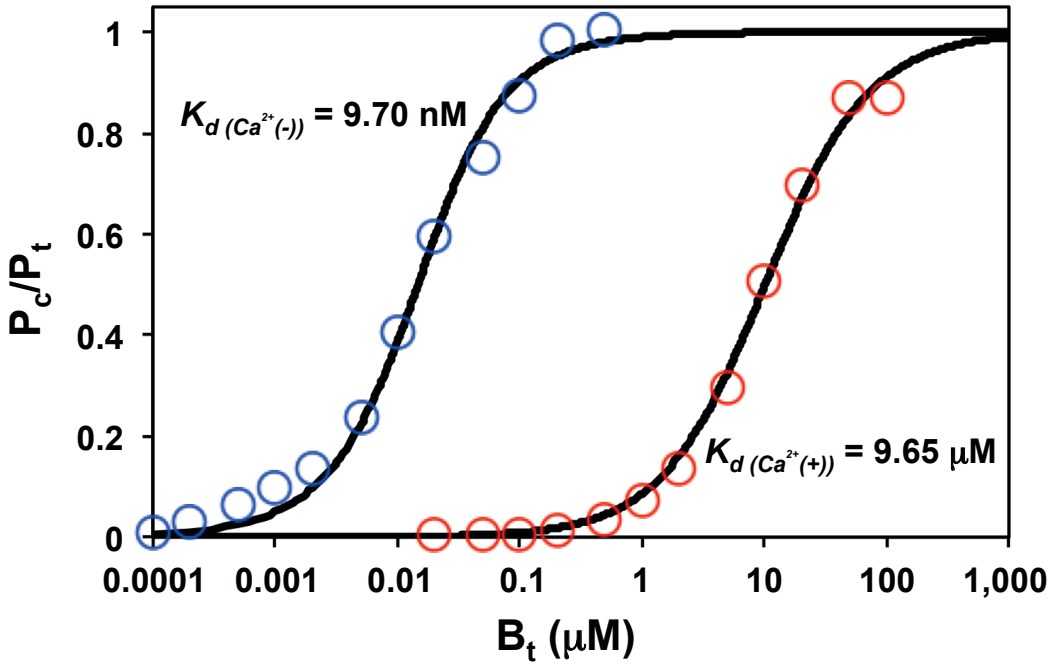

Figure 3.5. One thousand-fold difference in affinity of BReleaCa for BR in the presence and absence of Ca^{2+}. Titrations of BReleaCa with BR in the presence (red) and absence (blue) of Ca^{2+}. The fraction of BR-BReleaCa (conjugated protein, P_c) to whole BReleaCa (total protein, P_t) was plotted. Reprinted with a modification and with permission from Yoh Shitashima, Togo Shimozawa, Toru Asahi, and Atsushi Miyawaki, A dual-ligand-modulable fluorescent protein based on UnaG and calmodulin, *Biochemical and Biophysical Research Communications*, 496, 872-879 (2018) [8], Elsevier, copyright 2018. Consent from all authors has been secured.

The derivation of the Equation (3.1)

The chemical equation for the concentrations of BR and BReleaCa in equilibrium state can be described as;

$$[BR]+[BReleaCa] \leftrightarrow [BR-BReleaCa] \Leftrightarrow K_d = \frac{[BR][BReleaCa]}{[BR-BReleaCa]}$$

Now, I define total concentration of BR (B_t), BReleaCa (P_t), and the concentration of conjugated protein (P_c) as;

$$B_t = [BR]+[BR-BReleaCa]$$
$$P_t = [BReleaCa]+[BR-BReleaCa]$$
$$P_c = [BR-BReleaCa]$$

Therefore, I obtain,

$$P_c = \frac{(K_d + B_t + P_t) - \sqrt{(K_d + B_t + P_t)^2 - 4 \cdot B_t \cdot P_t}}{2}$$

Herein, I define the parameter *A*, which is the value of FI that BR assumes binding to all BReleaCa. The relationship between brightness and concentration of protein is described as;

$$\frac{FI}{A} = \frac{P_c}{P_t}$$

where FI indicates the experimental FI for titration. Finally, I can estimate the value of K_d by analyzing the Fi value with the function using K_d and *A* as parameters. The equation is described as;

$$FI = \frac{(K_d + B_t + P_t) - \sqrt{(K_d + B_t + P_t)^2 - 4 \cdot B_t \cdot P_t}}{2 \cdot P_t} \cdot A$$

3.3.4 The association and dissociation rate constant of BReleaCa and BR

Next, I investigated the effects of Ca^{2+}-binding on the association/dissociation kinetics of BR to BReleaCa. I first determined the association rate (k_{on}) of BR on BReleaCa. I performed stopped-flow analysis by mixing 1 μM BReleaCa and 1 μM BR in the absence of free Ca^{2+} ion, and focused on the rapid phase of the FI increase to determine the $k_{on\ (Ca^{2+}(-))}$ value to be 8.04×10^5 $M^{-1}s^{-1}$ (Figure 3.6A). I did the same measurement in the presence of Ca^{2+} ion, and determined the $k_{on\ (Ca^{2+}(+))}$ value to be 1.99×10^3 $M^{-1}s^{-1}$ (Figure 3.6B).

I then analyzed the kinetics of dissociation of BR from BR-BReleaCa in both Ca^{2+}(-) and Ca^{2+}(+) pathways using UnaG(N57A). As this mutant of UnaG binds to BR with the same affinity as the wild-type but is a nearly non-fluorescent, it can be used as a quick scavenger of BR [9]. Under a Ca^{2+}-depleted condition, I monitored FI during the conversion from BR-BReleaCa to BReleaCa (Figure 3.4) after the addition of an excess amount of UnaG(N57A). The FI of a solution containing 10 nM BR-BReleaCa decayed exponentially after the addition of N57A (~500 nM) (Figure 3.6C), and the dissociation rate constant ($k_{off\ (Ca^{2+}(-))}$) was determined to be 1.09×10^{-2} s^{-1}. Because of an extremely low abundance of the Ca^{2+}-BR-BReleaCa species, on the other hand, the BR dissociation process under a Ca^{2+}-saturated condition (Figure 3.4) is hard to analyze. So, I started FI measurement from the highly fluorescent species, BR-BReleaCa. After the simultaneous addition of $CaCl_2$ with UnaG(N57A), I should be able to monitor the FI during the conversion toward BReleaCa via Ca^{2+}-BR-BReleaCa. Based on the fact that the association between Ca^{2+} and CaM is extremely fast (~10^8 $M^{-1}s^{-1}$) [15], the FI decay was analyzed to determine an apparent value of the dissociation rate constant $k'_{off\ (Ca^{2+}(+))}$

to be 2.09×10^{-2} s^{-1} (Figure 3.6D). These measurements regarding BR binding are summarized in Table 3.1.

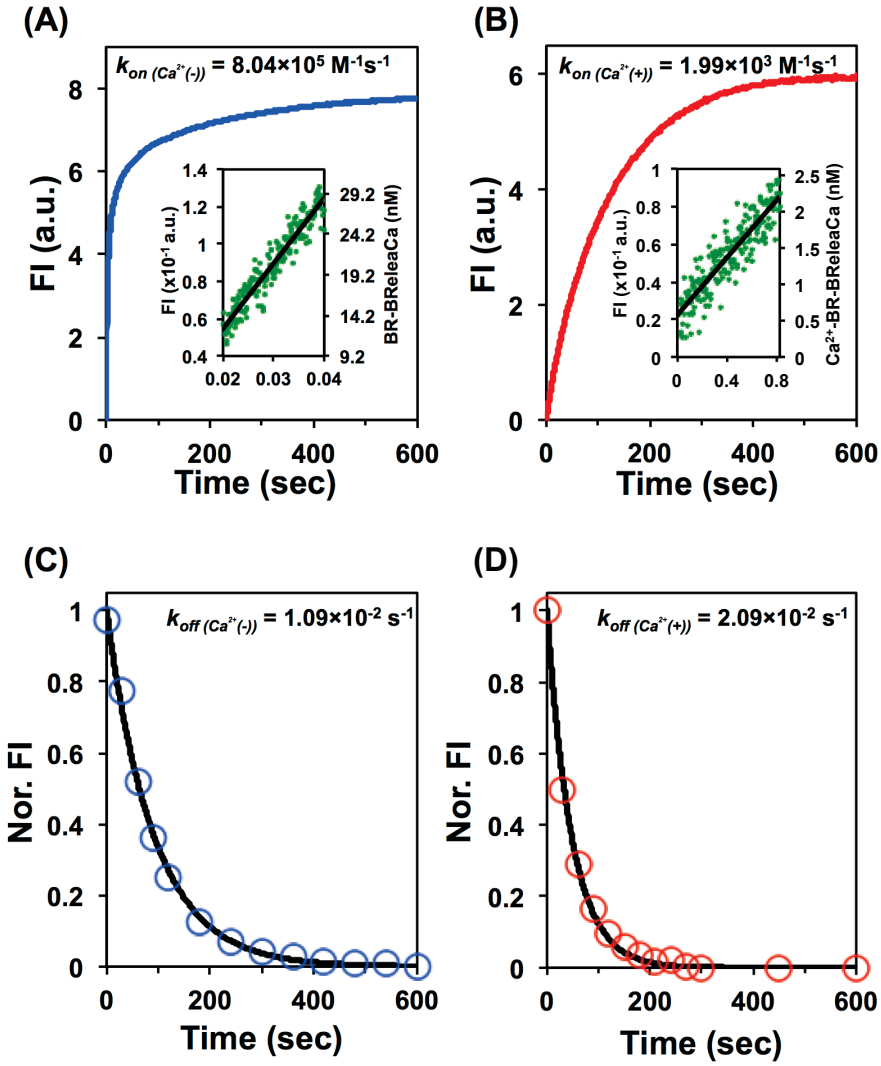

Figure 3.6. Kinetics of BR binding of BReleaCa. (**A, B**) The time-courses of the intensity of fluorescence after the addition of BR (1 μM) to BReleaCa (1 μM) in the Ca^{2+}-free (A, blue curve) and Ca^{2+}-saturated (B, red curve) states. (**A, B, insets**) The time-courses in the very early phase (green circles) with the best-fitting lines are shown. The right axis of ordinate shows calculated concentrations of BR-BReleaCa (see the materials and methods section). (**C, D**) The time-courses of the intensity of fluorescence from BR-BReleaCa (~10 nM) after the addition of 50-fold excess (500 nM) of apoN57A in the absence (C, blue) and presence (D, red) of Ca^{2+} ion. Best-fitting curves are drawn in black. Reprinted with a modification and with permission from Yoh Shitashima, Togo Shimozawa, Toru Asahi, and Atsushi Miyawaki, A dual-ligand-modulable fluorescent protein based on UnaG and calmodulin, *Biochemical and Biophysical Research Communications*, 496, 872-879 (2018) [8], Elsevier, copyright 2018. Consent from all authors has been secured.

Table 3.1 Dissociation constant and kinetic rate constants

Sample	K_d (M)	k_{on} (M^{-1} s^{-1})	k_{off} (s^{-1})
UnaG WT[8, 13]	9.80×10^{-11}	7.05×10^{6}	2.17×10^{-4}
BReleaCa (Ca^{2+}(−))	9.70×10^{-9}	8.04×10^{5}	1.09×10^{-2}
BReleaCa (Ca^{2+}(+))	9.65×10^{-6}	1.99×10^{3}	2.09×10^{-2}

Reprinted with permission from Yoh Shitashima, Togo Shimozawa, Toru Asahi, and Atsushi Miyawaki, A dual-ligand-modulable fluorescent protein based on UnaG and calmodulin, *Biochemical and Biophysical Research Communications*, 496, 872-879 (2018) [8], Elsevier, copyright 2018. Consent from all authors has been secured.

3.3.5 Performance of BReleaCa expressed in cultured mammalian cells

I performed a Ca^{2+} titration experiment in the presence of an excess amount of BR, and determined the K_d of BR-BReleaCa for Ca^{2+} binding to be 0.82 μM (Figure 3.7) by using equation 3.2 (see the derivation of the equation 3.2).

$$FI_{nor} = \frac{-\left(K_{dCa^{2+}} + Ca_t^{2+} - P_t\right) + \sqrt{\left(K_{dCa^{2+}} + Ca_t^{2+} - P_t\right)^2 + 4 \cdot K_{dCa^{2+}} \cdot P_t}}{2 \cdot P_t} \quad \cdots \text{Equation (3.2)}$$

$$+\alpha \cdot \frac{\left(K_{dCa^{2+}} + Ca_t^{2+} + P_t\right) - \sqrt{\left(K_{dCa^{2+}} + Ca_t^{2+} + P_t\right)^2 - 4 \cdot Ca_t^{2+} \cdot P_t}}{2 \cdot P_t}$$

K_d of BR-BReleaCa for Ca^{2+} binding is much higher than the resting level of intracellular free Ca^{2+} concentration ($[Ca^{2+}]_i$) of mammalian cell types. I fused BReleaCa to mCherry and transfected the resultant chimeric protein (BReleaCa-mCherry) into cultured HeLaS3 cells. I substituted Hank's balanced salt solution without calcium (HBSS(-)) and with 100 μM EGTA for the growth medium. I also added 100 nM BR to the HBSS(-). I found that transfected cells emitted green as well as red fluorescence, suggesting that BReleaCa folded well enough for BR incorporation, and that considering the $K_{d\ (Ca^{2+}(-))}$ value for BR binding (9.70 nM) and high cell permeability of BR, the folded molecules existed exclusively as BR-BReleaCa.

I increased $[Ca^{2+}]_i$ by addition of 1 μM ionomycin together with 1 mM $CaCl_2$ (Figure 3.8A, *top*, time = 0) and found a decrease in the green fluorescence. However, the addition of 2 mM EGTA-Na (t = 10 min.) restored the green fluorescence to some extent (Figure 3.8A, *top*). During the time period, the red fluorescence was quite stable (Figure 3.8A, *middle*), and I plotted the ratio of green fluorescence intensity to the red

one (Figure 3.8B), which demonstrates that BReleaCa functions as the dual-ligand fluorescent protein in mammalian cell types.

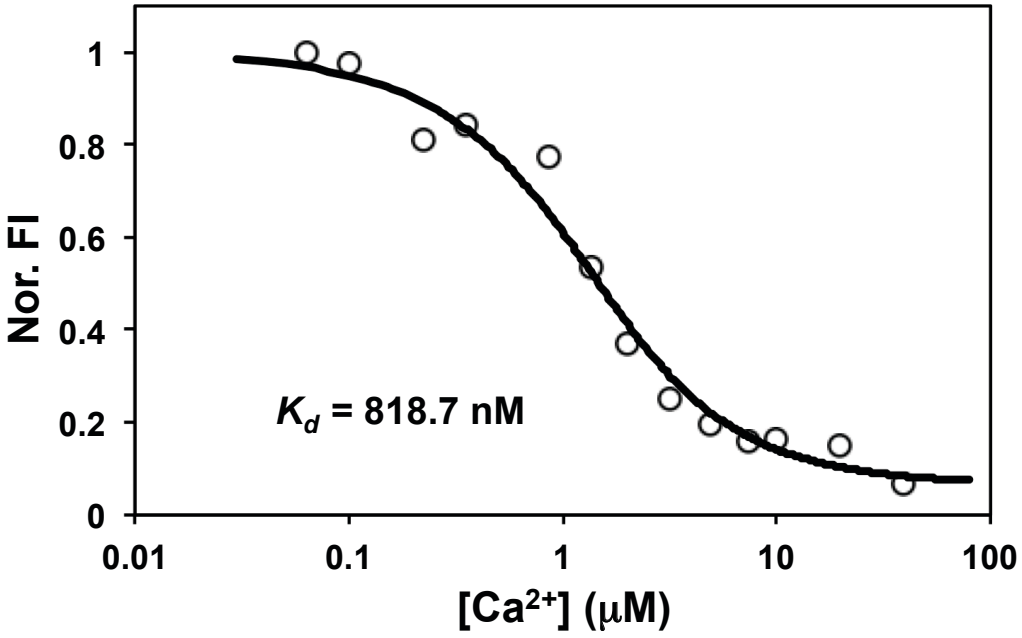

Figure 3.7. Titration of BR-BReleaCa with calcium using Calcium Calibration Buffer Kit #1. Each 1 μM BReleaCa solution containing various concentrations of free Ca^{2+} ions (from 0.064 to 39 μM) was incubated at 20°C until measurement. Each sample was measured at 5 min from the addition of excess BR (200 μM). Reprinted with permission from Yoh Shitashima, Togo Shimozawa, Toru Asahi, and Atsushi Miyawaki, A dual-ligand-modulable fluorescent protein based on UnaG and calmodulin, *Biochemical and Biophysical Research Communications*, 496, 872-879 (2018) [8], Elsevier, copyright 2018. Consent from all authors has been secured.

The derivation of the Equation (3.2)

The chemical equation for the concentrations of Ca^{2+} and BR-BReleaCa in equilibrium state can be described as;

$$\left[Ca^{2+}\right]+\left[BR-BReleaCa\right]\leftrightarrow\left[Ca^{2+}-BR-BReleaCa\right]\Leftrightarrow K_{dCa^{2+}}=\frac{\left[Ca^{2+}\right]\left[BR-BReleaCa\right]}{\left[Ca^{2+}-BR-BReleaCa\right]}$$

In this situation, I should describe both the concentration of BR-BReleaCa and Ca^{2+}-BR-BReleaCa using P_t and $Ca^{2+}{}_t$ (total Ca^{2+} concentration) because both BR-BReleaCa and Ca^{2+}-BR-BReleaCa exhibit fluorescent properties. The concentration of BR-BReleaCa and Ca^{2+}-BR-BReleaCa can be described as;

$$\left[BR-BR\mathrm{e}leaCa\right]=\frac{-\left(K_{dCa^{2+}}+Ca_t^{2+}-P_t\right)+\sqrt{\left(K_{dCa^{2+}}+Ca_t^{2+}-P_t\right)^2+4\cdot K_{dCa^{2+}}\cdot P_t}}{2}$$

$$\left[Ca^{2+}-BR-BR\mathrm{e}leaCa\right]=\frac{\left(K_{dCa^{2+}}+Ca_t^{2+}+P_t\right)-\sqrt{\left(K_{dCa^{2+}}+Ca_t^{2+}+P_t\right)^2-4\cdot Ca_t^{2+}\cdot P_t}}{2}$$

The brightness of BR-BReleaCa and Ca^{2+}-BR-BReleaCa were expressed as 1 and α, respectively, the normalized FI is represented by

$$FI_{nor}=\frac{-\left(K_{dCa^{2+}}+Ca_t^{2+}-P_t\right)+\sqrt{\left(K_{dCa^{2+}}+Ca_t^{2+}-P_t\right)^2+4\cdot K_{dCa^{2+}}\cdot P_t}}{2\cdot P_t}$$

$$+\alpha\cdot\frac{\left(K_{dCa^{2+}}+Ca_t^{2+}+P_t\right)-\sqrt{\left(K_{dCa^{2+}}+Ca_t^{2+}+P_t\right)^2-4\cdot Ca_t^{2+}\cdot P_t}}{2\cdot P_t}$$

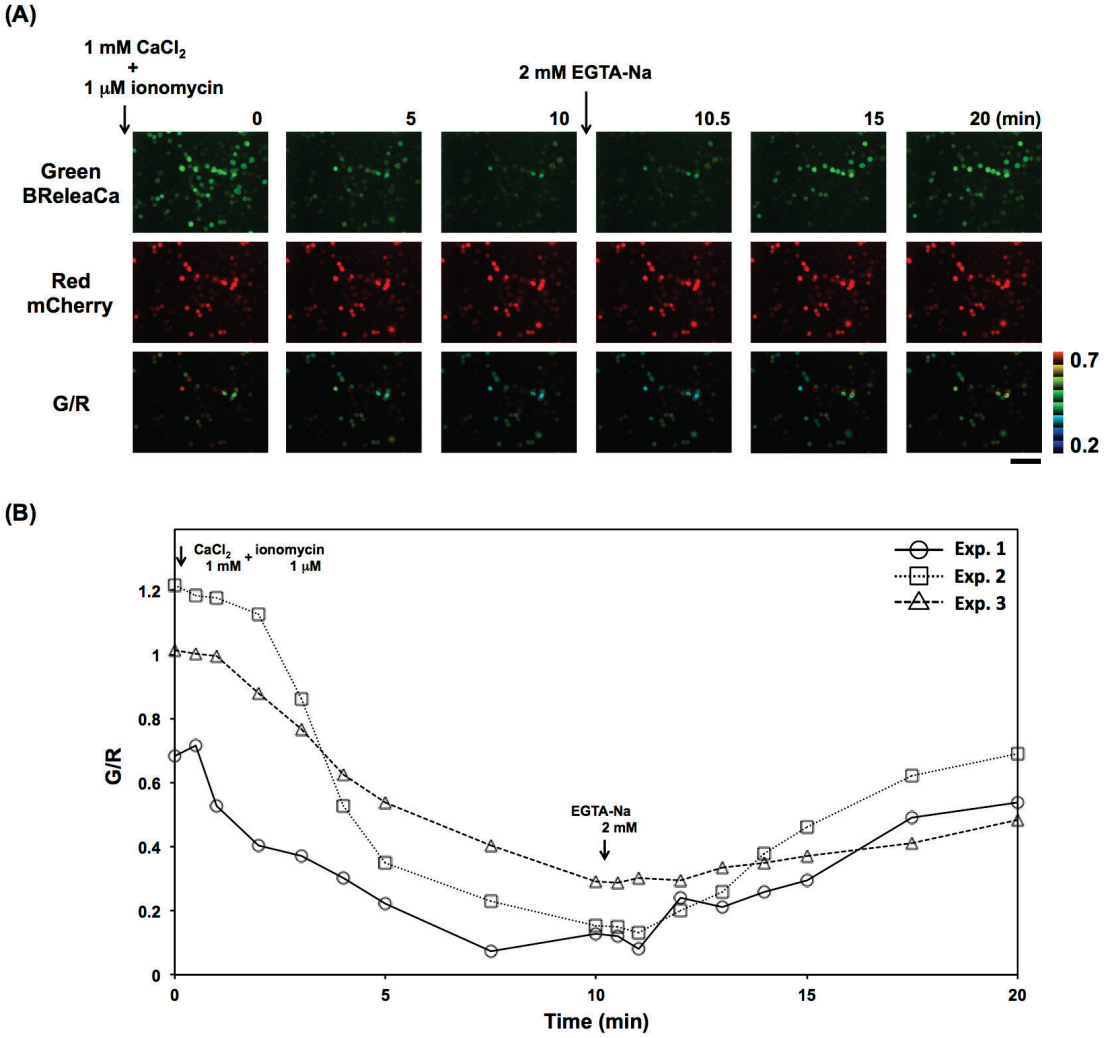

Figure 3.8. Ca^{2+}-regulated fluorescence of BReleaCa in HeLa S3 cells. HeLa cells were transfected with the cDNA of BReleaCa-mCherry fusion, and time-lapse imaged. (A) *top*, Decrease in the BReleaCa green fluorescence after the addition of 1 mM $CaCl_2$ and 1 μM ionomycin at 0 min, and its recovery after the addition of 2 mM EGTA-Na at 10 min. *middle*, The mCherry red fluorescence was nearly constant. *bottom*, Ratio images of green to red. Scale bar, 100 μm. (B) Time courses of the ratio of the green fluorescence to the mCherry red fluorescence from three independent experiments. Typical images selected from Exp. 1 are presented in (A). Reprinted with permission from Yoh Shitashima, Togo Shimozawa, Toru Asahi, and Atsushi Miyawaki, A dual-ligand-modulable fluorescent protein based on UnaG and calmodulin, *Biochemical and Biophysical Research Communications*, 496, 872-879 (2018) [8], Elsevier, copyright 2018. Consent from all authors has been secured.

3.4 Discussion

3.4.1 Challenging of other type of BR releasing protein

To offer Ca^{2+} sensitivity to a BR-inducible fluorescent protein, in this study, I constructed 6 UnaG/CaM hybrid proteins. After affinity tag purification of bacterially expressed proteins and reconstitution with BR, I measured absorption spectra of their Ca^{2+}-free form (Figure 3.9). Among the 6 hybrid proteins, only #3 folded well enough to bind BR and exhibited light absorption peaking sharply at 494 nm. Moreover, the holoUnaG-derived absorption peak at 494 nm was reversibly sensitive to Ca^{2+} ion. In contrast, the 494- nm absorption peak was never detected with #1, and although the peak was very faintly observed for #2, #4, #5 and #6, none of them responded to Ca^{2+} ion. With preparations of #1, #2, #4, #5, and #6, furthermore, I noticed that the transmittance was substantially reduced irrespective of the wavelength, and thus suspected their aggregation due to misfolding. Taken together, their failure in folding could be simply explained by UnaG's intolerance of the insertions.

A number of genetically encoded calcium indicators have been developed by introducing a cleft on the wall of the β-can fold of *Aequorea* GFP variants. On the one hand, most of the SFPBI, including G-CaMP, GCaMP, and pericam, are chimeric constructs that fuse circularly permuted variants of *Aequorea* GFP, such as cp145GFP and cp145YFP, to CaM and the CaM-binding peptide of myosin light-chain kinase (M13) [5, 16, 17]. So far, however, I have not been able to fuse cp85UnaG to CaM and M13 for our purpose (#5 and #6). More trial and error will be required to optimize protein integrity (folding efficiency). On the other hand, Camgaroo was successfully constructed by inserting only CaM between positions 145 and 146 of YFP [6]. Likewise, successful insertion between positions 84 and 85 of UnaG was achieved with CaM (#3)

but not CaM-M13 (#4) in our current study.

#3 appeared to ensure correct folding of both of the 2 protein modules: UnaG and CaM. In the present study, I investigated the interplay between the BR-induced development of green fluorescence and Ca^{2+} -induced conformational change on the protein. As #3 binds BR to become fluorescent and releases BR in response to Ca^{2+} ion, I named the protein "BReleaCa". The Ca^{2+} -free form "BR-BReleaCa" (Figure 3.4) emitted very bright green fluorescence. I compared absorption, excitation and fluorescence spectra between UnaG and BReleaCa (Figure 3.10), and I quantified its molar extinction coefficient (62,400 $M^{-1}cm^{-1}$) and fluorescence quantum yield (0.40), which were comparable to those of the wild-type UnaG (77,300 $M^{-1}cm^{-1}$ and 0.51, respectively) (Table 3.2).

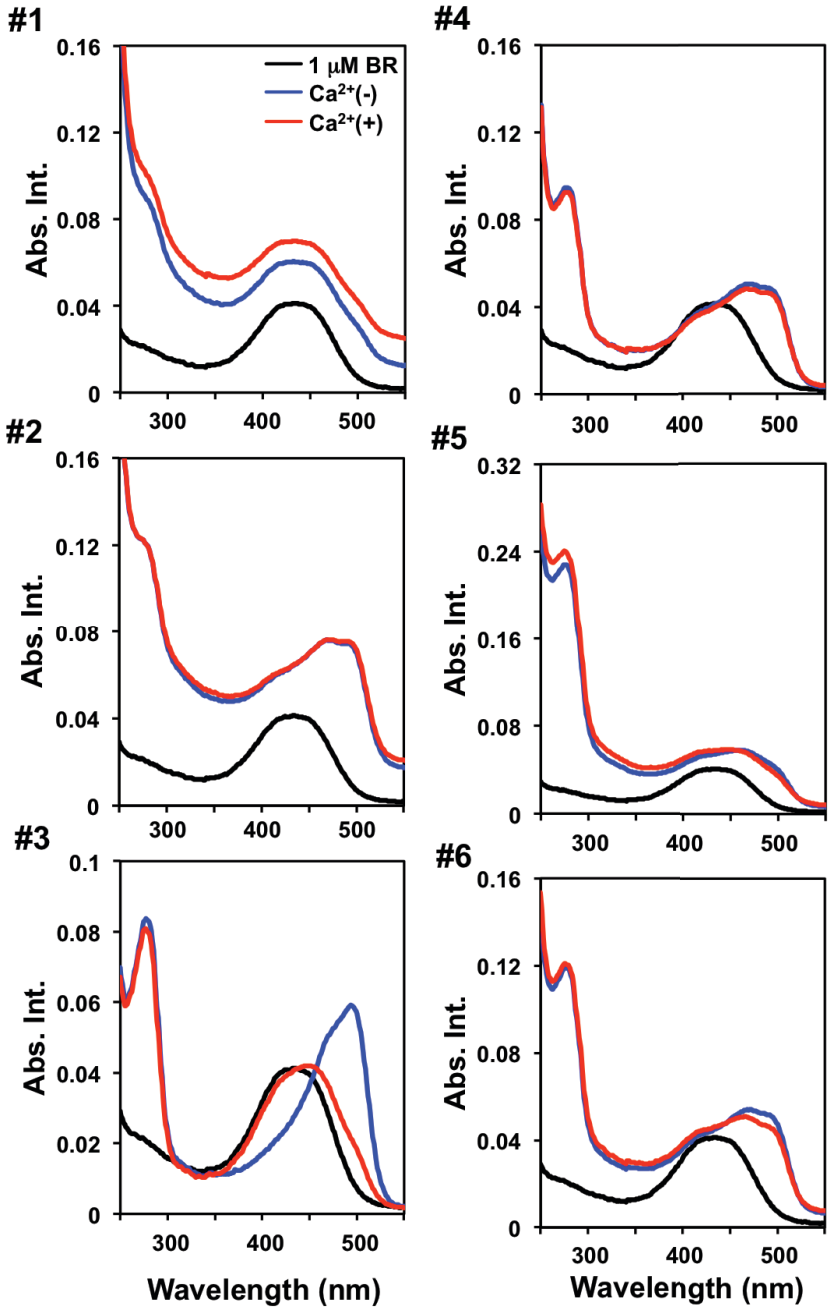

Figure 3.9. Absorption spectra of UnaG/CaM hybrid proteins. In all experiments, 1 μM BR and 100 μM EGTA-Na were added in each protein solution (1 μM) before measurement. Black line; Absorption spectra of 1 μM BR. Absorption spectra of #1 (A), #2 (B), #3 (BReleaCa, C), #4 (D), #5 (E), and #6 (F) chimeric protein before (blue line) and after (green line) addition of 200 μM $CaCl_2$. Reprinted with a modification and with permission from Yoh Shitashima, Togo Shimozawa, Toru Asahi, and Atsushi Miyawaki, A dual-ligand-modulable fluorescent protein based on UnaG and calmodulin, *Biochemical and Biophysical Research Communications*, 496, 872-879 (2018) [8], Elsevier, copyright 2018. Consent from all authors has been secured.

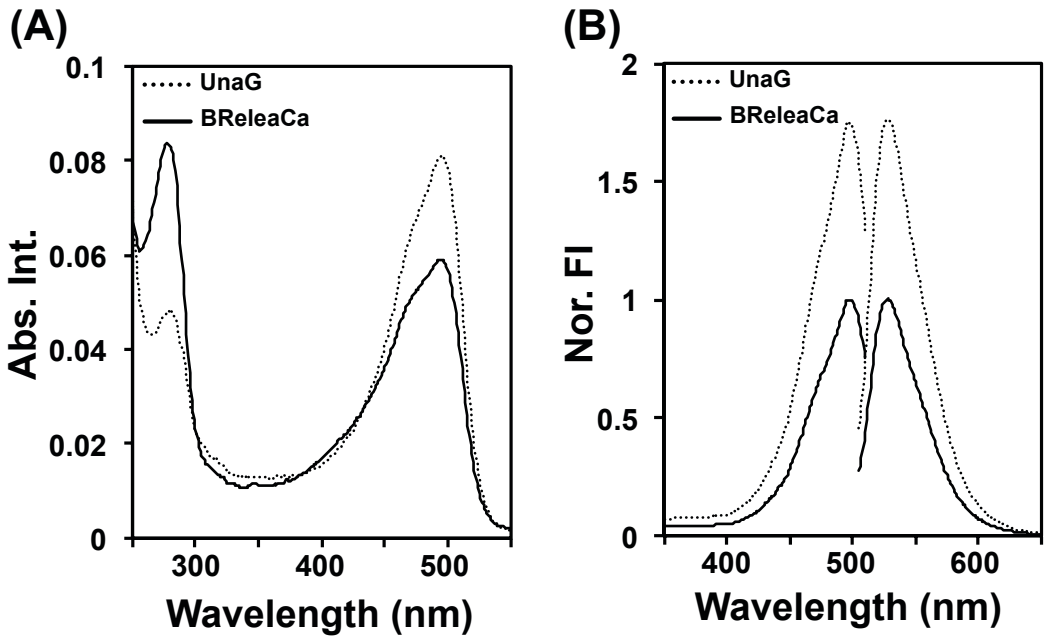

Figure 3.10. Spectroscopic studies for comparing UnaG and BReleaCa. (A) Absorption spectra of UnaG (dotted line) and BReleaCa (solid line) in the absence of Ca^{2+} (Ca^{2+}(-)). 1 μM BR and 100 μM EGTA-Na were added in UnaG and BReleaCa (1 μM each) protein solution. (B) Excitation and fluorescence spectra of UnaG (dotted line) and BReleaCa (black line) (1 μM each) with 1 μM BR and 100 μM EGTA-Na (Ca^{2+}(-)). Reprinted with permission from Yoh Shitashima, Togo Shimozawa, Toru Asahi, and Atsushi Miyawaki, A dual-ligand-modulable fluorescent protein based on UnaG and calmodulin, *Biochemical and Biophysical Research Communications*, 496, 872-879 (2018) [8], Elsevier, copyright 2018. Consent from all authors has been secured.

Table 3.2 Fluorescence characteristics od UnaG and BR-BReleaCa

	ex/em maxima (nm)	Molar extinction coefficient ($M^{-1}cm^{-1}$)	Fluorescence quantum yield
UnaG[13]	498/527	77,300 (498 nm)	0.51
BReleaCa (Ca^{2+}(-))	498/527	62,400 (498 nm)	0.40

Reprinted with permission from Yoh Shitashima, Togo Shimozawa, Toru Asahi, and Atsushi Miyawaki, A dual-ligand-modulable fluorescent protein based on UnaG and calmodulin, *Biochemical and Biophysical Research Communications*, 496, 872-879 (2018) [8], Elsevier, copyright 2018. Consent from all authors has been secured.

Additionally, I attempted to insert CaM into cpUnaG (cpBReleaCa). CaM was inserted between the original N and C terminus, and N terminus of cpBReleaCa starts at the amino acid residue 85 position and the C terminus ends at residue 84. Although cpBReleaCa exhibited some responses to Ca^{2+}, this BR releasing protein could not bind completely 1 μM BR in the Ca^{2+}-free state, indicating that the K_d value between cpBReleaCa and BR under a Ca^{2+}-depleted condition would larger than that between BReleaCa and BR. Moreover, I attempted to change the insertion position of CaM, in place between residues 24 and 25, or in place between residues 57 and 58. The position in the former is inter two α-helix and the position in the latter is near the key amino acid Arg57 [9, 13]; needless to say, both position are very close to BR binding pocket in UnaG. Although both BR releasing protein exhibited some responses to Ca^{2+}, they could not release completely 1 μM BR in the Ca^{2+}-saturated state, indicating that the K_d value between these proteins and BR in the Ca^{2+}-saturated state would larger than that between BReleaCa and BR. In both cases, the differences of BR binding affinities for these proteins between the absence and presence of excess Ca^{2+} are expected to be smaller than that for original BReleaCa.

From these facts, I believe that original BReleaCa is currently the best designed BR releasing protein based on UnaG.

3.4.2 Consideration of portal region of UnaG from BReleaCa

Based on the view that the rate constants of association and dissociation of a ligand are largely related to the portal region and binding cavity, respectively, I discuss observed alterations of the kinetics of BR binding in two steps: insertion and conformational change of CaM. First, in the absence of Ca^{2+} ion, the insertion of apoCaM at 84/85 resulted in a ~100-fold decrease in the affinity of UnaG for BR (K_d, 9.80×10^{-11} M vs. 9.70×10^{-9} M). Because residues 84 and 85 are localized close to the propionate group protruding from the C ring of BR, the insertion should increase the rate constant of BR dissociation; the $k_{off\,(Ca^{2+}(-))}$ value of BReleaCa (1.09×10^{-2} s^{-1}) was approximately 100 times greater than the k_{off} of UnaG (2.17×10^{-4} s^{-1}). Second, the conversion from apoCaM to holoCaM upon binding to Ca^{2+} ion might cause some conformational change within the UnaG moiety, probably affecting the entry region for BR to a greater extent than the binding cavity. According to this speculation, $k_{on(Ca^{2+}(+))}$ (1.99×10^{3} $M^{-1}s^{-1}$) was approximately 400 times lower than $k_{on(Ca^{2+}(-))}$ (8.04×10^{5} $M^{-1}s^{-1}$), while $k_{off\,(Ca^{2+}(+))}$ (2.09×10^{-2} s^{-1}) was just a double of the $k_{off\,(Ca^{2+}(-))}$ value.

3.4.3 The possibility of utilizing BReleaCa

I determined the fluorescence quantum efficiency (QE) of BReleaCa to be 0.4, which is comparable to that of UnaG (0.51). It is possible that BReleaCa can be used as a transient binder of the fluorogenic ligand, bilirubin, for super-resolution imaging. The molar ratio of the bright bound state to non-fluorescent states can be controlled by Ca^{2+} ions according to object density. Further studies, including single molecule analysis of BReleaCa at different Ca^{2+} concentrations, will be necessary.

3.5 Conclusion

In conclusion, I have succeeded in rationally designing a Ca^{2+}-dependent bilirubin releasing protein, BReleaCa, based on the insertion of conformationally sensitive receptors into a ligand-binding protein. The resultant protein bound to BR with a K_d value of 9.70 nM in the Ca^{2+}-free state, and with a K_d value of 9.65 μM in the Ca^{2+}-saturated state. In kinetics study, the difference in BR binding affinities for BReleaCa in the absence and presence of excess Ca^{2+} was dominated by the difference of k_{on} rather than that difference of k_{off}. Moreover, The BR releasing ability of the novel created protein also functioned in cells; therefore, BReleaCa may be promising as a Ca^{2+}-inducible regulator of BR concentrations in biological tissues.

The strategy in this study may be widely applicable as a method of modulating protein-ligand affinity by using distinct molecules. Additionally, insertions of various foreign proteins in the site between residues 84 and 85 provide UnaG with expansions of dynamic range for BR sensing in cells. Furthermore, BReleaCa may contribute to super-resolution imaging field in the future. This study opens wider possibilities for UnaG application.

3.6 References

1. Vítek, L., "Bilirubin and atherosclerotic diseases", *Physiol Res*, **66**, S11–S20 (2017).
2. (UK), N. C. C. for W. and C. H., *Neonatal Jaundice*, *Neonatal Jaundice*, (2010).
3. Stocker, R., Y. Yamamoto, A. F. McDonagh, A. N. Glazer, and B. N. Ames, "Bilirubin is an antioxidant of possible physiological importance", *Science*, **235**, 1043–6 (1987).
4. Sedlak, T. W., and S. H. Snyder, "Bilirubin benefits: cellular protection by a biliverdin reductase antioxidant cycle", *Pediatrics*, **113**, 1776–82 (2004).
5. Miyawaki, A. and Y. Niino, "Molecular Spies for Bioimaging-Fluorescent Protein-Based Probes", *Molecular Cell*, **58**, 632–643 (2015).
6. Baird, G. S., D. A. Zacharias, and R. Y. Tsien, "Circular permutation and receptor insertion within green fluorescent proteins", *Proc. Natl. Acad. Sci. U. S. A.*, **96**, 11241–11246 (1999).
7. To, T. L., Q. Zhang, and X. Shu, "Structure-guided design of a reversible fluorogenic reporter of protein-protein interactions", *Protein Sci.*, **25**, 748–753 (2016).
8. Shitashima, Y., T. Shimozawa, T. Asahi, and A. Miyawaki, "A dual-ligand-modulable fluorescent protein based on UnaG and calmodulin", *Biochem. Biophys. Res. Commun.*, **496**, 872-879 (2018).
9. Shitashima, Y., T. Shimozawa, A. Kumagai, A. Miyawaki, and T. Asahi, "Two distinct fluorescence states of the ligand-induced green fluorescent protein UnaG", *Biophys. J.*, **113**, 2805-2814 (2017).
10. Zhang, Y., U. Werling, and W. Edelmann, "SLiCE: A novel bacterial cell

extract-based DNA cloning method", *Nucleic Acids Res.*, **40**, e55 (2012).

11. Motohashi, K. "A simple and efficient seamless DNA cloning method using SLiCE from Escherichia coli laboratory strains and its application to SLiP site-directed mutagenesis", *BMC Biotechnol.*, **15**, 47 (2015).
12. Zou, J., A. M. Hofer, M. M. Lurtz, G. Gadda, A. L. Ellis, N. Chen, Y. Huang, A. Holder, Y. Ye, C. F. Louis, K. Welshhans, V. Rehder, and J. J. Yang, "Developing sensors for real-time measurement of high Ca^{2+} concentrations", *Biochemistry*, **46**, 12275–12288 (2007).
13. Kumagai, A., R. Ando, H. Miyatake, P. Greimel, T. Kobayashi, Y. Hirabayashi, T. Shimogori, and A. Miyawaki, "A bilirubin-inducible fluorescent protein from eel muscle", *Cell*, **153**, 1602–1611 (2013).
14. Heinemann, U. and M. Hahn, "Circular permutation of polypeptide chains: implications for protein folding and stability", *Prog. Biophys. Mol. Biol.*, **64**, 121-143 (1995).
15. Kubota, Y., J. A. Putkey, and M. N. Waxham, "Neurogranin controls the spatiotemporal pattern of postsynaptic Ca^{2+}/CaM signaling", *Biophys. J.*, **93**, 3848–59 (2007).
16. Nakai, J., M. Ohkura, and K. Imoto, "A high signal-to-noise Ca^{2+} probe composed of a single green fluorescent protein", *Nat. Biotechnol.*, **19**, 137–41 (2001).
17. Nagai, T., A. Sawano, E. S. Park, and A. Miyawaki, "Circularly permuted green fluorescent proteins engineered to sense Ca^{2+}", *Proc. Natl. Acad. Sci. U. S. A.*, **98**, 3197–3202 (2001).

Chapter 4

Summary and Future Prospect

In this thesis, the characteristic of UnaG and its novel application were studied. The former study is summarized in Chapter 2 and the latter is summarized in Chapter 3.

In Chapter 2, the most remarkable achievement is discovering that holoUnaG is the mixture of two distinctive fluorescent molecules by using fluorescence intensity distribution analysis (FIDA). The trigger of this discovery was careful observation of FI-time course for measuring the association/dissociation rates of UnaG and BR. The time-dependent green fluorescence of apoUnaG upon addition of BR was investigated, and I finally identified that the holoUnaG solution immediately showed strong brightness (rapid phase), and subsequently the fluorescence intensity gradually increased to a plateau (slow phase). From both the fitting analysis of FI time-course in show phase under various UnaG concentrations and the result of analytical ultracentrifugation analysis, the slow FI increase was associated with an intra-molecular reaction within the already formed holoUnaG molecule. To clarify this hypothesis, I subjected holoUnaG to FIDA. Finally, I demonstrated that apoUnaG was converted to holoUnaG$_1$ immediately, and subsequently holoUnaG$_1$ was gradually converted to holoUnaG$_2$, which acquired 3.9 times higher brightness than holoUnaG$_1$. Both holoUnaG$_1$ and holoUnaG$_2$ reached equilibrium state with an average holoUnaG$_1$/holoUnaG$_2$ ratio of 60:40. From these results, I suggested the novel schema for the formation of the UnaG and BR complex system, and determined the various rate constants including the association/dissociation rates of UnaG and BR. The finding in Chapter 2 provided useful information for the application of UnaG. And, the idea of utilizing FIDA instead of single-molecular imaging is my own original method. This

method would be apply for the analysis of other fluorescence protein, so I think my study would give high impact in this field.

In Chapter 3, I offered the Ca^{2+} sensitivity to UnaG via a genetic insertion of a calmodulin (CaM) domain. The originality of this study is the idea of regulating the affinity of ligand binding by using other molecule. The resultant protein decreased its affinity for BR by ~1,000-fold by increasing Ca^{2+} ion concentration. Moreover, I calculate the quantum yield of BReleaCa and it was estimated to be 0.4. This value is relatively high for fluorescent protein quantum yield, indicating that BReleaCa is suitable element for single-molecular imaging. I believe that my findings will open the possibility for UnaG application of UnaG as an element for super-resolution imaging in the future. The strategy in this study may be widely applicable as a method for generating intentional changes to protein-ligand affinity. Thus, I strongly assert that this study represents a significant contribution to researchers in the protein-engineering field.

For future prospect, there are several possibilities in my study. For example, nobody knows which dipyrrinone moieties exhibit fluorescence properties. Possibly, one-sided dipyrrinone moieties may exhibit fluorescence properties in holoUnaG$_1$, and both dipyrrinone moieties may exhibit fluorescence properties in holoUnaG$_2$. I would like to separate holoUnaG$_1$ from holoUnaG$_2$ completely in the future. For this challenge, I have to determine the difference between holoUnaG$_1$ and holoUnaG$_2$ at first. I would like to determine the key residue for playing a role of transition between holoUnaG$_1$ and holoUnaG$_2$, and finally achieve to generate the super-UnaG whose QE is ~90%. In BReleaCa, I would like to utilize BReleaCa as a functional element *in vitro*, like DNA-origami. For example, BReleaCa has a potential to be a useful labelled protein for

point accumulation for imaging in nanoscale topography (PAINT) as described in Chapter 3. If we utilize BReleaCa for PAINT, fluorescent densities would be easily controlled by Ca^{2+} ion. The study in this thesis will open the possibility of UnaG as a useful protein, and lead to create various novel functional protein based on fluorescent protein (Figure 4.1).

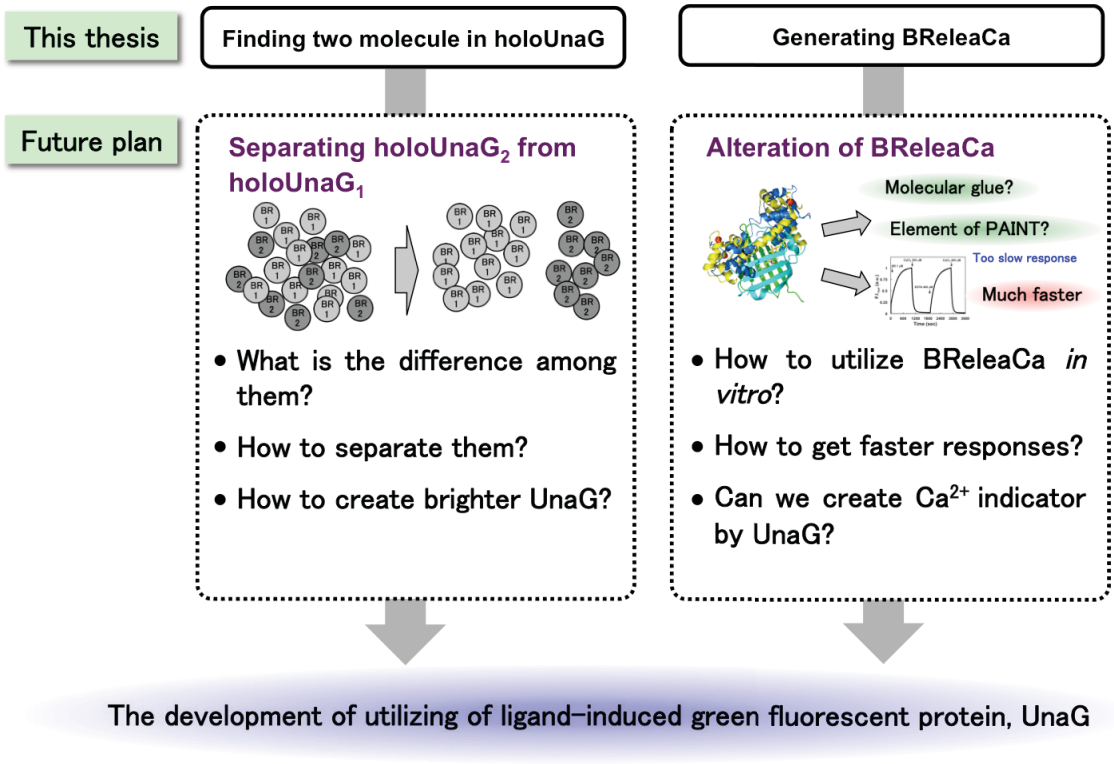

Figure 4.1. Prospects for future research of UnaG.

Acknowledgements

This study is carried out with my supervisor Prof. Dr. Toru Asahi, who belongs to Department of Life Science and Medical Bioscience Department of Advanced Science and Engineering in Waseda University. I joined his laboratory in 2015, from my doctoral course. I would like to be deeply grateful to him for his kind supervision on my work. He always took thought for me, even if he pressed by his works. I am very glad to join his laboratory.

In the final year in my doctoral course, I could do my research at RIKEN. I would like to appreciate with sincere gratitude to Dr. Atsushi Miyawaki. I really want to focus on “optical property” and “protein science” in doctoral course, and fluorescent protein is a good theme for me. Dr. Atsushi Miyawaki is known as one of the authorities of fluorescent protein, and I am very honor to join his laboratory in the final year in my doctoral course. He gave me his precious time and discussed the application of UnaG and BReleaCa, although he was always very busy. I am very fortunate to join his laboratory, and I am obliged to him for acceptance me in the final year in my doctoral course. Besides him, I wish to thank Prof. Dr, Teruo Fujii in Institute of Lndustrial Science, the University of Tokyo, because he introduced me to Dr. Atsushi Miyawaki.

In writing this thesis, I would like to express my deepest appreciation to my great mentor, Dr. Togo Shimozawa in Waseda University (now in Tokyo University). In three years, he always leads me with strict but appropriate direction as a researcher; for example, data analyzing, writing academic papers logically, deeply consideration for experiments, the change of viewpoint and so on. He always makes time to direct me. I always respect him about his way of thinking as a researcher, and I would like to be a scientist with logical consideration and multifaceted perspectives for natural science

like him.

I am very grateful to Prof. Dr. Kuniki Kino in Waseda University and Dr. Toshiki Furuya in Waseda University (now in Tokyo University of Science) for leading me in my bachelor's and master's course. They directed me the fundamental of research in my undergraduate, and they also taught me the interest of protein engineering through enzymatic engineering. Thanks to them, I was very interested in natural science.

I would like to thank to Prof. Dr. Etsuro Ito in Waseda University and Mr. Masashi Mita in Shiseido Co., Ltd. They evaluated my doctoral thesis and gave me several instructive comments.

I would like to also thank to Dr. Akiko Kumagai in RIKEN. Dr. Atsushi Miyawaki and she provided UnaG gene.

I am also glad to lab-members and staffs in Asahi Laboratory, especially, Dr. Yoshiyuki Ogino, Dr. Akifumi Takanabe, Dr. Satoru Wakabayashi for deeply discussion about this thesis. I could conduct my doctoral study with their help, sharing information, and sometimes idle chatting. I also thank lab-members in Miyawaki Laboratory and Kino Laboratory. I am glad to my friends in Waseda University and doctoral colleagues in leading graduate program in other universities.

Finally, I would like to say thanks for my family, my father, my mother and my brother. Thanks to their continuous support, I could conduct my Ph. D. study smoothly. When I was very sad and painful, they always understood me and encourage me. Thanks again for my luck that my lovely family surrounds me.

February 2018

Yoh Shitashima

Research Achievements

Publications

○1. Yoh Shitashima, Togo Shimozawa, Toru Asahi, and Atsushi Miyawaki, "A dual-ligand-modulable fluorescent protein based on UnaG and calmodulin", *Biochem. Biophys. Res. Commun.*, **496**, 872-879 (2018).

○2. Yoh Shitashima, Togo Shimozawa, Akiko Kumagai, Atsushi Miyawaki, and Toru Asahi, "Two distinct fluorescence states of the ligand-induced green fluorescent protein UnaG", *Biophys. J.*, **113**, 2805-2814 (2017).

3. Toshiki, Furuya, Yoh Shitashima, and Kuniki Kino, "Alteration of the substrate specificity of cytochrome P450 CYP199A2 by site-directed mutagenesis", *J. Biosci. Bioeng.*, **119**, 47-51 (2015).

Presentations

(International, Poster)

1. Yoh Shitashima, Togo Shimozawa, and Toru Asahi, “Equilibrium of Two Fluorescence States in The UnaG-Bilirubin Complex”, Biophysical Society 61st Annual Meeting, 2877-Pos B484, Ernest N. Morial Convention Center, New Orleans, February 2017.
2. Yoh Shitashima, Togo Shimozawa, Miyabi Ishida, and Toru Asahi, "Chiroptical Properties of the Bilirubin Compounded with Fluorescent Protein UnaG *in vitro* ", Pacifichem2015, 07BIOL-133, Hawaii Convention Center, Honolulu, December 2015.

(Domestic, Oral)

1. 下島洋, 下澤東吾, 石田みやび, 朝日透, “蛍光特性を用いたビリルビン依存型蛍光タンパク質UnaGの自己二量化の解析”, 日本化学会第96春季年会, 2C4-05B, 同志社大学, 2016年3月
2. 下島洋, 古屋俊樹, 木野邦器, “酵素-基質間の静電的相互作用に着目したシトクロムP450酸化酵素CYP199A2の基質特異性改変”, 日本化学会第94春季年会, 3G5-09A, 名古屋大学, 2014年3月

(Domestic, Poster)

1. 下島洋, 下澤東吾, 石田みやび, 朝日透, “Billirubin依存型蛍光タンパク質UnaGのキラル特性解析”, Symposium on Molecular Chirality 2015, P-056, 早稲田大学, 2015年6月
2. 下島洋, 古屋俊樹, 木野邦器, “基質-酵素間相互作用を担う官能基の交換によるP450モノオキシゲナーゼCYP199A2の基質特異性改変”, 第17回生体触媒化学シンポジウム, 1P-05, 岡山理科大学, 2013年12月
3. 下島洋, 古屋俊樹, 木野邦器, “シトクロムP450酸化酵素CYP199A2の立体構造に基づいた基質特異性の改変”, 第3回CSJ化学フェスタ2013, P5-92, タワーホール船堀, 2013年10月

Others

(Awards)

1. 第24回生物工学論文賞, Toshiki Furuya, Yoh Shitashima, and Kuniki Kino, “Alteration of the substrate specificity of cytochrome P450 CYP199A2 by site-directed mutagenesis”, *J. Biosci. Bioeng.*, **119**, 47-51 (2015)、2016年5月
2. 優秀ポスター発表賞, 下島洋, 古屋俊樹, 木野邦器, “シトクロムP450酸化酵素CYP199A2の立体構造に基づいた基質特異性の改変”, 第3回CSJ化学フェスタ2013, P5-92, タワーホール船堀, 2013年10月
3. Gold Award, 下島洋, 辻理絵子, 橋香奈, 水口佳紀, 安田翔也, “OYAKonnect~保育園に通う子どもの興味・友達関係が分かるシステム~”, EDGE INNOVATION CHARENGE COMPETITION 2015, 東京, 2015年2月

(Commentary)

1. 古屋俊樹, 下島洋, 木野邦器, “部位特異的変異導入によるシトクロムP450 CYP199A2の基質特異性改変”, 生物工学会誌, 第95巻, 第2号, 71 (2017).

(Research Funding)

1. 2015年度三菱マテリアル-理工学術院研究助成金（30万円）, 下島洋, 2015年7月